Large-scale Circulation Departures Related to Wet Episodes in Northeast Brazil

Dhirendra N. Sikdar and James B. Elsner

Atmospheric Sciences Division

Dept. of Geological/Geophysical Sciences

University of Wisconsin-Milwaukee

Milwaukee, WI 53211

USA

October 1985

SUMMARY

Large-scale circulation features are presented as related to wet spells over northeast Brazil (Nordeste) during the rainy season (March and April) of 1979. The rainy season is divided into dry and wet periods, for which we have averaged the FGGE and geostationary satellite data and studied mean and departure fields of basic variables and cloudiness. Analysis of seasonal mean circulation features show: lowest sea level pressures SLP's over the Amazon basin and along the equator; low and middle level easterlies beneath upper level westerlies; weak meridional winds; high relative humidity over the Amazon basin and relatively dry conditions over the South Atlantic Ocean. Departure characteristics for the wet periods include: positive cloud anomaly over Nordeste; strong negative SLP departures (1-2mb) over the South Atlantic; significant 850 mb zonal wind decrease over southern Nordeste, positive temperature departures at upper levels, probably due to latent heating; and positive relative humidity departures.

The vertical profiles of mean variables over Nordeste indicate: (i) veering of wind with height, (ii) mean descending motions throughout the troposphere, and (iii) convective stability below 850 mb. The departure profiles exhibit: (i) weak low and middle level easterlies for wet episodes, (ii) high variability of meridional wind suggesting wave propagation in the zonal flow, (iii) strong upward motion and a large positive moisture departure nearly at all levels.

In summary, we found a fluctuation in the large-scale circulation features on time scales of a few weeks or so over Nordeste and the South Atlantic sector during March and April of 1979. Even the subtropical High SLP's have large departures during wet episodes, implying a short period oscillation in the southern hemisphere Hadley circulation.

1. INTRODUCTION

The drought/flood phenomenon of northeast Brazil (hereafter referred to as Nordeste) has widespread serious sociological and economical consequences. Rainfall over Nordeste is highly variable both in space and time, however, there are distinct rainy seasons. Northern Nordeste's rainy season (primarily the states of Maranhao, Piaui, Ceara, Rio Grande Do Norte, Paraiba, Pernambuco, and Algoa) is centered, but not confined to, the months of March and April and is related to the meridional position of the lower tropospheric confluence zone over the tropical Atlantic. For the south (primarily the states of Sergipe, Bahia, and northern Minas Gerais), yearly maxima occur in November and December. Agriculture in the north is geared for planting in December and January and harvesting in May. If drought or floods occur in March and/or April, crops are ruined.

Over the past couple of decades, numerous studies examining various circulation patterns associated with rainfall variability over Nordeste have been done (Namias, 1972; Hastenrath, 1976; Hastenrath and Heller, 1977; Kousky, 1979; Moura and Shukla, 1981; Chu, 1983, 1984; and Hastenrath, 1984). However, the concern of these investigations has been large-scale circulation patterns related to drought and flood years over Nordeste. At present, knowledge of circulation patterns related to wet and dry episodes within a particular rainy season is far from complete, mainly due to lack of adequate observations on this time scale. This gap has recently been narrowed by the special observing systems-satellite, ships, buoys and aircraft-taken during the operational phase of the Global Weather Experiment. The data collected and processed in the form of FGGE level IIIb grids allows for extensive diagnosis of large-scale circulation components on a daily basis.

The object of this study is to examine relationships of cloudiness, moisture, SLP and winds over Nordeste and the adjacent Brazil-Atlantic sector to

rainfall episodes over northern Nordeste during March and April of 1979. The experiment divides the rainy season (March and April) into wet and dry days, then composites variables with respect to persistent rainfall episodes. Spatial fields (Part A) and vertical profiles (Part B) of seasonal means as well as wet departures are analyzed. Results are compared to studies of annual variability.

2. DATA SOURCE AND ANALYSIS TECHNIQUES

Winds, moisture and SLP's from FGGE level IIIb along with bright (cold) cloud estimates from GOES-EAST constitute the main data base. Monthly rainfall totals for stations in Nordeste were obtained from Monthly Climatic Data for the World. Daily rainfall totals were received from both the National Climatic Data Center in Asheville, NC and from the Superintendencia de Desenvolvimento do Nordeste in Recife, Pernambuco, Brazil.

Cloud amounts are estimated in 5 degree lat-long areas from infrared full disk pictures for the region bounded by 20°N to 20°S and 20°W to 70°W. Estimates are made three times daily at 0000, 1200 and 1800 GMT for all of March and April. On occasion the 0000 or 1200 GMT picture is missing, in which case the 0600 GMT picture is substituted. The estimating procedure excludes cloudiness which appears dull gray to the eye. The possible effect of this low brightness cutoff is to exclude cloud regions consisting primarily of stratus or small cumulus. Cloud amounts are then averaged to obtain daily means.

Daily means of the other variables are calculated from the 0000 and 1200 GMT grids. Spatial grids of daily mean upper-air variables at 200, 500 and 850 mb along with SLP's are used in this study. Latitude and longitude bounds are set at 30°N to 30°S and 60°W to 15°E respectively. For the daily mean vertical profiles, area of averaging is approximately 520,000 km^2 and covers 20 grid points of data over Nordeste. Nine mandatory levels are available starting at

1000 mbs.

Two stations with 30 year rainfall climatological records were available within the study region. Both stations indicated negative departures of rainfall for March and April of 1979. Quixerambim and Barra Do Corrda received only 47 and 32 percent of their normal March and April total precipitation respectively.

Initially the rainy season is divided into wet and dry episodes. This is accomplished using daily rainfall totals for stations over Nordeste. Ten stations are uniformly distributed within the dry region of northern Nordeste (Fig. 1). Table (I) gives the station name, earth coordinates, elevation above sea level and WMO number. Averaging criteria are based on the following. A day is marked as wet if it meets either one of the following two conditions, (1) more than two stations within the dry region with recorded rainfall (1 mm or more), (2) less than three stations with recorded rainfall, but total precipitation greater than 10 mm. If the day does not meet either criterion it is marked as dry. As a further specification, in order to isolate rainfalls associated with pronounced weather systems, only days within a precipitation event (either wet or dry) of three successive days or longer are used for averaging. In this way, only rainfalls accompanying more persistent weather systems are identified. All composite departure fields and profiles are based on these criteria. Figure 2 is a histogram plot of the normalized rainfall departures with wet episodes identified. As a way to put the rainfall during March and April into seasonal perspective, Table (II) shows the ten station mean monthly percentages of total yearly rainfall for 1979 along with standard deviations. January through May have the largest mean percentages, with March and April of these five months having the smallest variations. This indicates that, as a whole March and April had relatively good spatial coverage of rainfall.

Sixty-one day means and departures of all spatial fields and vertical profiles were computed. All spatial fields except bright cloud amount are subject to a 25 point smoothing filter. No vertical smoothing is used. Results are presented in section three and summerized in section four.

3. RESULTS

(a) Spatial fields

(i) Seasonal means

Percent bright cloud amounts are shown in Fig. 3. Minimum cloudiness (less than 30%) associated with the subtropical highs are found north of 5°N and south of the equator. Maximum cloudiness (greater than 40%) is found over the Amazon basin and between the equator and 5°N over the tropical Atlantic associated with the lower tropospheric confluence axis. Seasonal mean SLP distribution is shown in Fig. 4. Lowest pressures are sandwiched between the subtropical high pressure regions of both hemispheres and extend from central Brazil to north of Nordeste and eastward to central Africa. Positions of SLP features for the rainy season of 1979 are in good agreement with the 61 year means for March and April (Hastenrath and Lamb, 1977). Also bright cloud amount and SLP show good spatial agreement.

Seasonal mean zonal winds (not shown) indicate, in general for the Atlantic tropical belt, easterlies at low and mid-levels with westerlies at upper levels (200 mb). Mean meridional winds are considerably weaker than the zonal current. At 200 mb (Fig. 5) a region of northerly winds is located to the east of Nordeste with a branch of southerlies over southern Brazil. This flow implies an upper level cyclonic circulation over Nordeste. The pattern at 850 mb indicates horizontal divergence, with southerlies over northern Nordeste and northerlies to the south of the region.

The seasonal mean temperature distributions (not shown) are rather

uninteresting at all three levels. However, the mean relative humidity field at 850 mb (Fig. 6) is noteworthy. Low relative humidities are noted over the eastern South Atlantic to the east of Nordeste. Highest humidities are associated with the tropical convergence zone over the Atlantic extending over north central Brazil. Therefore, since the mean zonal low-level winds are easterly, the flow over the eastern South Atlantic is from a region of low relative humidities toward a region of higher humidities. Our moisture analysis from the level IIIb data agrees reasonably well with the dewpoint analysis of Newton (1972).

(ii) Composite departures

Departure patterns of bright cloud amount for wet composites are shown in Fig. 7. Positive departures for wet episodes were expected since cumulus convection is the principle precipitation mechanism of the region (Ramos, 1975). However the region of negative departures over the Amazon suggests that rainfall over Nordeste may be regulated by the intensity of deep convection over that region (Silva Dias, et. al., 1983). Composite departures of SLP's (Fig. 8) indicate a relative weakening of the South Atlantic High (SAH) and a relative strengthening of the North Atlantic High (NAH) during wet episodes. The weakening or strengthening may be due to a latitudinal displacement of the pressure systems. Figure 9 clearly shows the difference of SLP south of the equator between wet composites and the mean. It is noted that, the departures in SLPs are of the same sign as those detected on the annual cycle (Hastenrath, et al, 1984).

Positive departures of 850 mb zonal wind (Fig. 10) for wet episodes over southern Nordeste and central Brazil extending over the eastern South Atlantic indicate weaker easterlies compared with the mean. Weak easterlies result in less moisture divergence (not shown) over Nordeste during wet episodes. As a further illustration, Fig. 11 shows composite meridional profiles of 850 mb

zonal wind, zonally averaged between 15° W and 60° W. The composite indicates substantially weaker easterlies between 5° S and 20° S latitude. This departure pattern is similar to the pattern detected on a yearly basis (Chu, 1983). The departure pattern of meridional wind is weak at both low and middle levels. At 200 mb strong positive departures are located over Nordeste and extend in a band northeastward to the coast of Africa (Fig 12). A region of negative departures is found to the west of this band. This suggests an influence of northern hemisphere mid-latitude frontal intrusions into the tropics near Africa on rainfall over Nordeste.

Temperature departures are generally very weak particularly near the equator. However at 200 mb a large region of positive departures is noted over Nordeste and central Brazil (Fig. 13). We have attributed this departure to latent heat release from cumulus convection. Relative humidity departures (not shown) over Nordeste are positive, as was expected. Since temperature departures are weak, higher relative humidities imply greater moisture over Nordeste compared with the mean.

(b) Vertical profiles

(i) Seasonal means

Profiles of mean zonal and meridional wind (not shown) indicate east and southeasterlies at low and middle tropospheres with southwesterlies above 300 mb. The profile of mean horizontal velocity divergence (Fig. 14) shows convergence in the lowest layer and also between 200 and 400 mb. Divergence dominates between 500 and 850 mb. Middle and low level divergence implies mean descending motions throughout much of the vertical. Mean descent over Nordeste is somewhat surprising since March and April are the rainy season. However, the time and space scale of averaging is several orders of magnitude larger than the scale of cumulus convection. Cumulus convection, as stated earlier, is the principle precipitation mechanism of the region. Subsidence over Nordeste at

this scale is an extension of the large-scale subsidence of the SAH which is centered near 30°S and 10°W during the northern hemisphere spring (Hastenrath and Lamb, 1977). The mean relative vorticity profile (not shown) indicates anticyclonic vorticity below the 200 mb level with cyclonic vorticity at 200 mb and above. Mean low level anticyclonic vorticity over Nordeste is a result of proximity to the SAH.

Based on the mean profile of air temperature (not shown) we found conditional stability between 850 and 1000 mb and instability above that to 400 mb. The mean profile of equivalent potential temperature indicates convective stability below 850 mb with convective instability between 400 and 850 mb. Data were averaged at approximately 0900 and 2100 local time, therefore, mean stability in the lowest layer does not accurately represent daytime stability over Nordeste.

From the vertical profile analysis it is clear that averaging over a large portion of Nordeste smooths the effects of smaller scales. Small scale circulations are directly related to cumulus precipitation. However, the effect of smaller scales can be enhanced by compositing data and computing departures.

(ii) Composite departures

Vertical profiles of departures are considerably more revealing than the mean profiles. Figure 15 depicts the profile of zonal wind departures. Since the mean zonal wind is easterly below 300 mb, positive departures indicate a weaker easterly flow over the region. Departures of meridional wind (not shown) are on the same order of magnitude as the mean component. This suggests high variability in space and time. Variability may be related to propagation of waves in the easterly current.

Figure 16 shows the vertical distribution of divergence departures. Departures are an order of magnitude smaller than the mean. Negative divergence departures below 700 mb indicate a stronger mean convergence at 1000 mb with a

weaker mean divergence at 850 mb. This situation is kinematically more favorable for precipitation than the mean state. These findings are consistent with Ramos (1975). Vertical profiles of omega departures are depicted in Fig. 17. Intensities of departures are approximately half the intensities of mean vertical motions. Negative departures for wet episodes indicate weaker subsidence which is expected, based on the divergence departures. Relative vorticity departures (not shown) are on the same order of magnitude as the mean values.

Temperature departures are extremely weak, in contrast, mixing ratio departures are relatively large. Figure 18 depicts vertical profiles of mixing ratio departures. Positive departures are noted throughout the vertical, indicating more environmental moisture than the mean state. Quantitatively this amounts to 4 to 5 percent more moisture during wet episodes when compared to the mean.

4. SUMMARY AND CONCLUSIONS

We have performed extensive analysis of atmospheric circulation components over Nordeste and the adjacent tropical Atlantic for March and April of 1979 using data accumulated during FGGE and processed by ECMWF in the form of twelve hourly grids. Sixty-one day means along with composite departures based on temporal and spatial rainfall distributions over northern Nordeste were computed for various circulation components. Results indicated that during the rainy season, Nordeste is located to the south and east of the ITCZ with its associated bright cloudiness and minimum surface pressures. To the north, the NAH is pronounced in both cloud and pressure fields. The SAH, located to the southeast of Nordeste produces east to southeasterly low level winds which blow onshore over Nordeste from the South Atlantic. Lower tropospheric air over the South Atlantic is relatively dry. Large-scale mean subsidence was found over

Nordeste and a large portion of the equatorial South Atlantic. Therefore, even during the rainy season the immediate environment over Nordeste is hostile towards precipitation.

Oscillations of certain meteorological variables were also detected. Large SLP departures were depicted during wet episodes. A relative intensification of the equatorward extension of the NAH along with a relative weakening of the equatorward extension of the SAH is clearly evident. This relative weakening of the SAH causes a slackening of lower tropospheric easterlies and concurrently a weakening of the moisture divergence over Nordeste. Further, no detectable latitudinal displacements of near-equatorial convergence and/or cloudiness were found in contrary to studies of interannual variability (Hastenrath, 1984). Anomalous upward motion is present over Nordeste during wet episodes. What we found then is circulation departures associated with rainfall over northern Nordeste within a particular rainy season are similar in some aspects to seasonal changes detected in the mean annual cycle. And it appears that rain/drought episodes even of a few days are defined in terms of certain large-scale circulation variations over the Brazil-Atlantic region.

ACKNOWLEDGMENTS

The authors wish to thank Drs. John Theon and Bob Curran for supporting this study through NASA grant no. NAG 5-384. A partial support for graduate students and computer usage came from the Graduate School.

REFERENCES

Chu, P. S. 1983 Diagnostic studies of rainfall anomalies in northeast Brazil, Mon. Weath. Rev., 111, 1655-1664.

1984 Time and space variability of rainfall and surface circulation in the Northeast Brazil-Tropical Atlantic sector, J. Meteor. Soc. Japan, 26, 363-369.

Hastenrath, S. 1976 Variations in low-latitude circulation and extreme climatic events in the tropical Americas, J. Atm. Sci., 33, 202-215.

1984 Interannual variability and annual cycle: mechanisms of circulation and climate in the tropical Atlantic sector. Mon. Weath. Rev., 112, 1097-1107.

Hastenrath, S. and Lamb, P. J. 1977 Climatic atlas of the tropical Atlantic and eastern Pacific Oceans, The University of Wisconsin Press, Madison, Wisconsin 53701. ISBN 0-299-07234-7.

Hastenrath, S. and Heller, L. 1977 Dynamics of climatic hazards in northeast Brazil. Quart. J. R. Met. Soc., 103, 77-92.

Hastenrath, S., Wu, M. C. and Chu, P. S. 1984 Towards the monitoring and prediction of northeast Brazil droughts, Quart. J. R. Met. Soc., 110, 411-425.

Kousky, V. E. 1979 Frontal influences on northeast Brazil. Mon. Weath. Rev., 107, 1140-1153.

Moura, A. D. and Shukla, J. 1981 On the dynamics of droughts in NE Brazil: observations, theory and numerical experiments with a general circulation model. J. Atm. Sci., 40, 2689-2707.

Namias, J. 1972 Influence of northern hemispher general circulation on drought in northeast Brazil. Tellus, 24, 336-343.

Newton, C. W. 1972 Meteorology of the southern hemisphere, American Meteorological Society, Chapter 6, 101-111.

Ramos, R. P. L. 1975 Precipitation characteristics in the northeast Brazil dry region. J. Geophys. Res., 80, 1665-1678.

Silva Dias, P. L., Schubert, W. H., and DeMaria, M. 1983 Large-scale response of the tropical atmosphere to transient convection. J. Atm. Sci., 40, 2689-2707.

Figure Legends

Figure 1. Regional map of northeast Brazil with isohyets of total rainfall for March and April 1979. Dry region is roughly delineated by the 200 mm isohyet. The ten stations used in the rainfall indexing are circled. FGGE level IIIb grid points are marked with an X.

Figure 2. Normalized rainfall departures of the ten stations within the dry region. Wet episodes are indicated with a bar below the graph.

Figure 3. Seasonal mean % bright cloud amount. Values are in whole percent.

Figure 4. Seasonal mean sea level pressure field. Values are 1000+ mb.

Figure 5. Seasonal mean 200 mb meridional wind field. Values are in ms^{-1}.

Figure 6. Seasonal mean 850 mb relative humidity field. Values are in whole percent.

Figure 7. Departure pattern of % bright cloud amount. Values are in whole percent.

Figure 8. Same as Fig. 7 except sea level pressures in mbs.

Figure 9. Meridional profiles of sea level pressures zonally averaged from 15° W to 60°W. Mean profile is solid and wet composite profile is dotted.

Figure 10. Same as Fig. 7 except 850 mb zonal wind in ms^{-1}.

Figure 11. Same as Fig. 9 except 850 mb zonal wind in ms^{-1}.

Figure 12. Same as Fig. 7 except 200 mb meridional wind in ms^{-1}.

Figure 13. Same as Fig. 7 except 200 mb temperatures in °C.

Figure 14. Vertical profile of seasonal mean horizontal velocity divergence. Values are $x10^{-6}$ s^{-1}.

Figure 15. Vertical profile of composite departures of zonal wind. Values are in ms^{-1}.

Figure 16. Same as Fig. 15 except horizontal divergence $x10^{-6}$ s^{-1}.

Figure 17. Same as Fig. 15 except omega $x10^{-5}$ mbs^{-1}.

Figure 18. Same as Fig. 15 except mixing ratio in gkg^{-1}.

Table I. Rainfall Stations

NAME	LAT.	LONG.	ELEV(m)	WMO #
Quixeramobim	04° 48′ S	39° 33′ W	250	82586
Crato	07° 02′ S	39° 29′ W	450	82784
Floriano	06° 52′ S	42° 52′ W	150	82678
Petrolina	08° 25′ S	40° 47′ W	500	82983
Paulo Alfonso	09° 35′ S	38° 13′ W	300	82986
Irece	10° 54′ S	41° 35′ W	450	83182
Teresina	05° 03′ S	42° 48′ W	70	82578
Bom Jesus	08° 46′ S	44° 24′ W	390	82975
Campina Grande	07° 19′ S	36° 01′ W	470	82795
Crateus	04° 56′ S	40° 45′ W	290	82583

Table II. Ten station mean monthly percentage of total yearly precipitation

MONTH	MEAN (mm)	S.D. (mm)
January	19.0	12.1
February	13.5	9.6
March	14.5	7.0
April	13.2	6.2
May	11.2	10.3
June	4.0	5.2
July	3.3	6.3
August	2.8	7.6
September	0.8	1.3
October	0.7	1.8
November	7.1	5.6
December	9.6	9.6

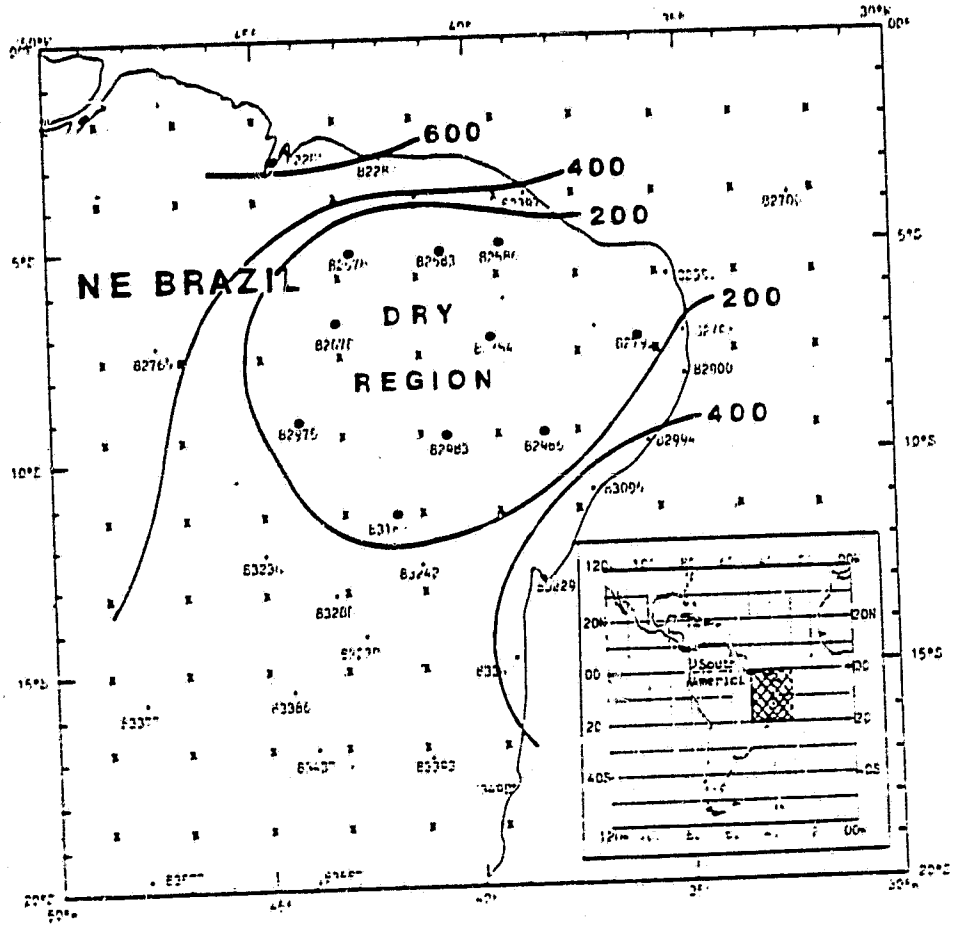

Fig. 1.

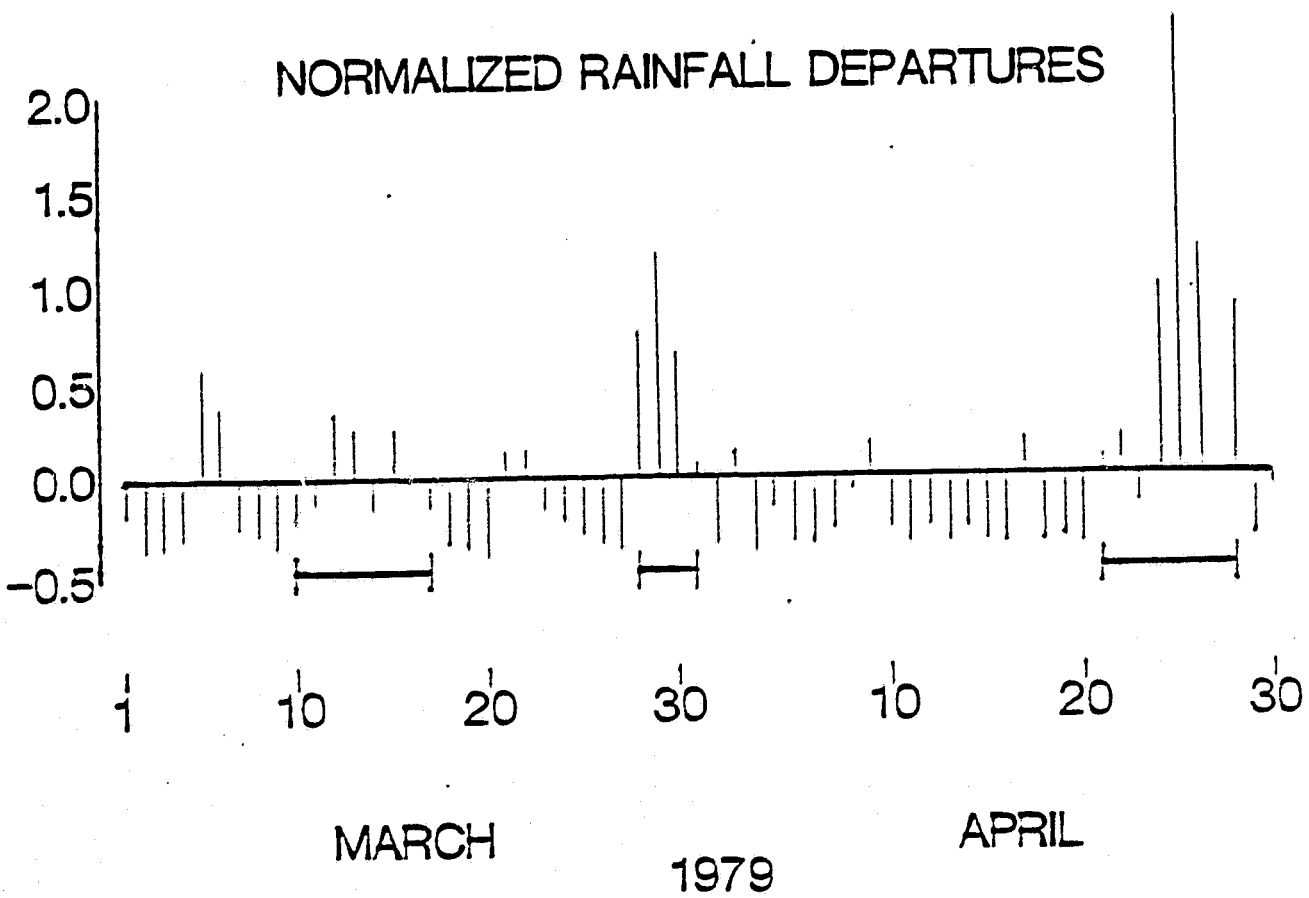
NORMALIZED RAINFALL DEPARTURES
2.0
1.5
1.0
0.5
0.0
-0.5
1
10
20
30
10
20
30
MARCH
APRIL
1979

Fig. 2.

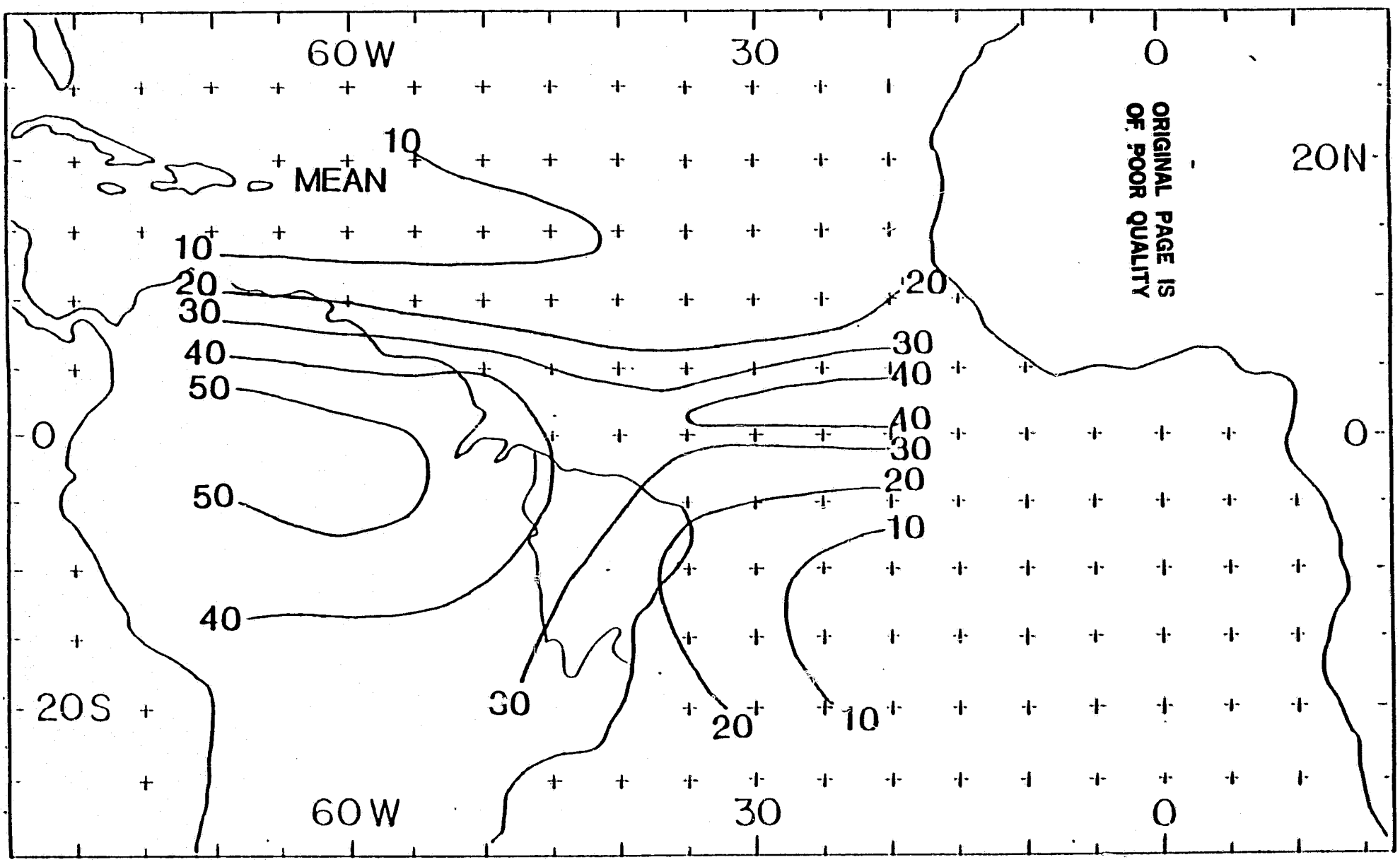
60W
30
0
20N
0
20S
MEAN
10
10
20
30
40
50
50
40
20
30
40
40
30
20
10
30
20
10
ORIGINAL PAGE IS
OF POOR QUALITY

Fig. 3

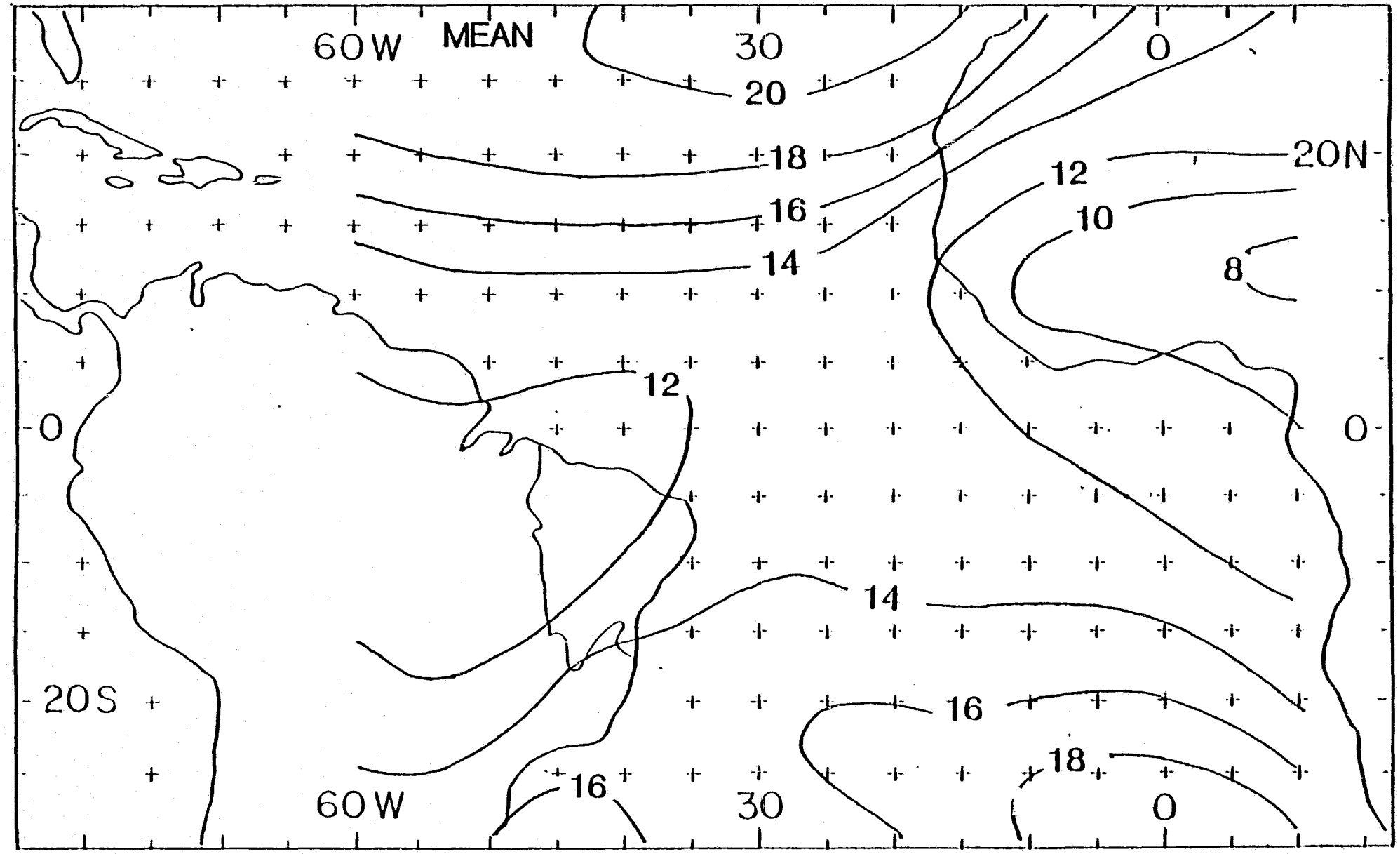

Fig. 4.

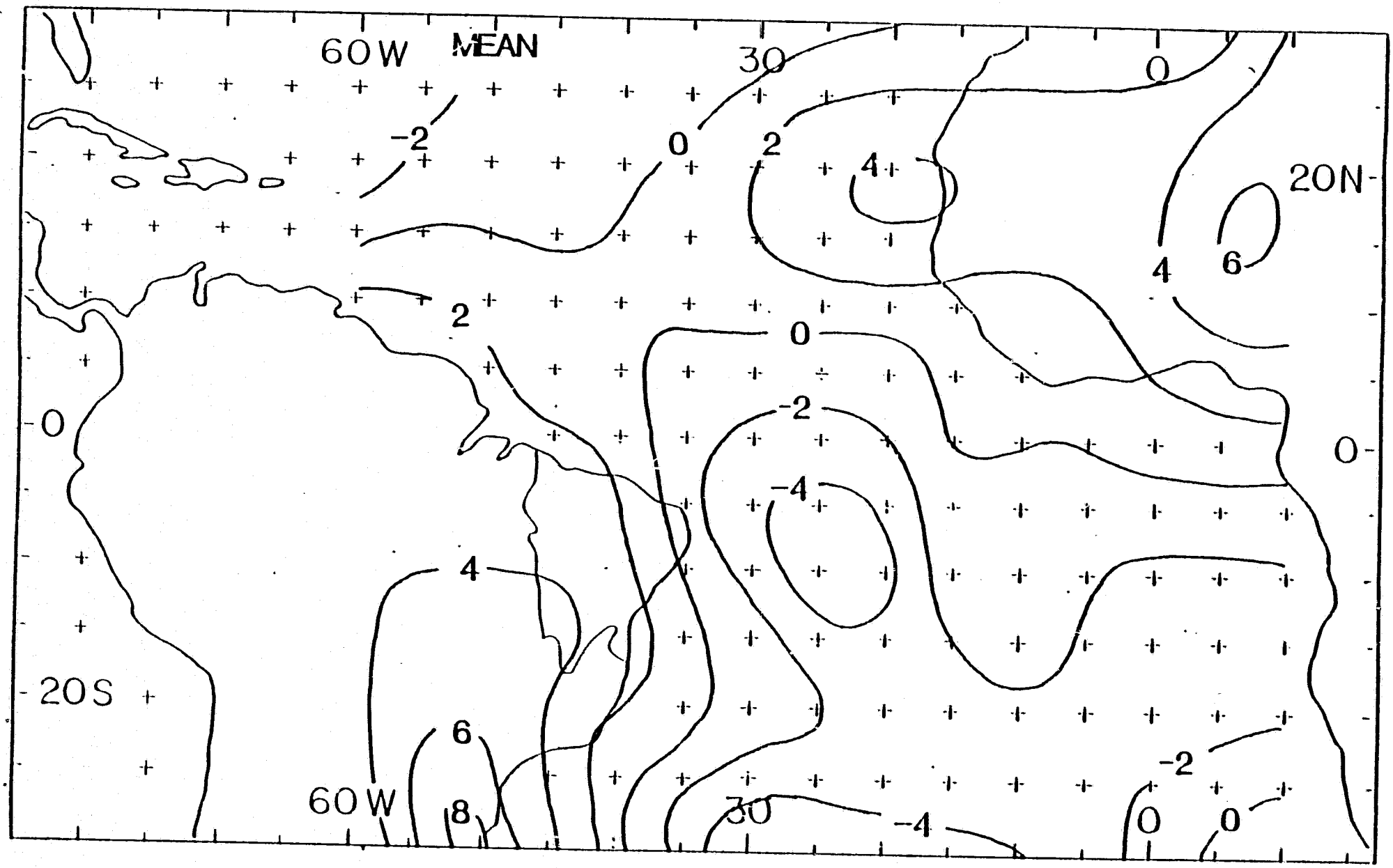

Fig. 5.

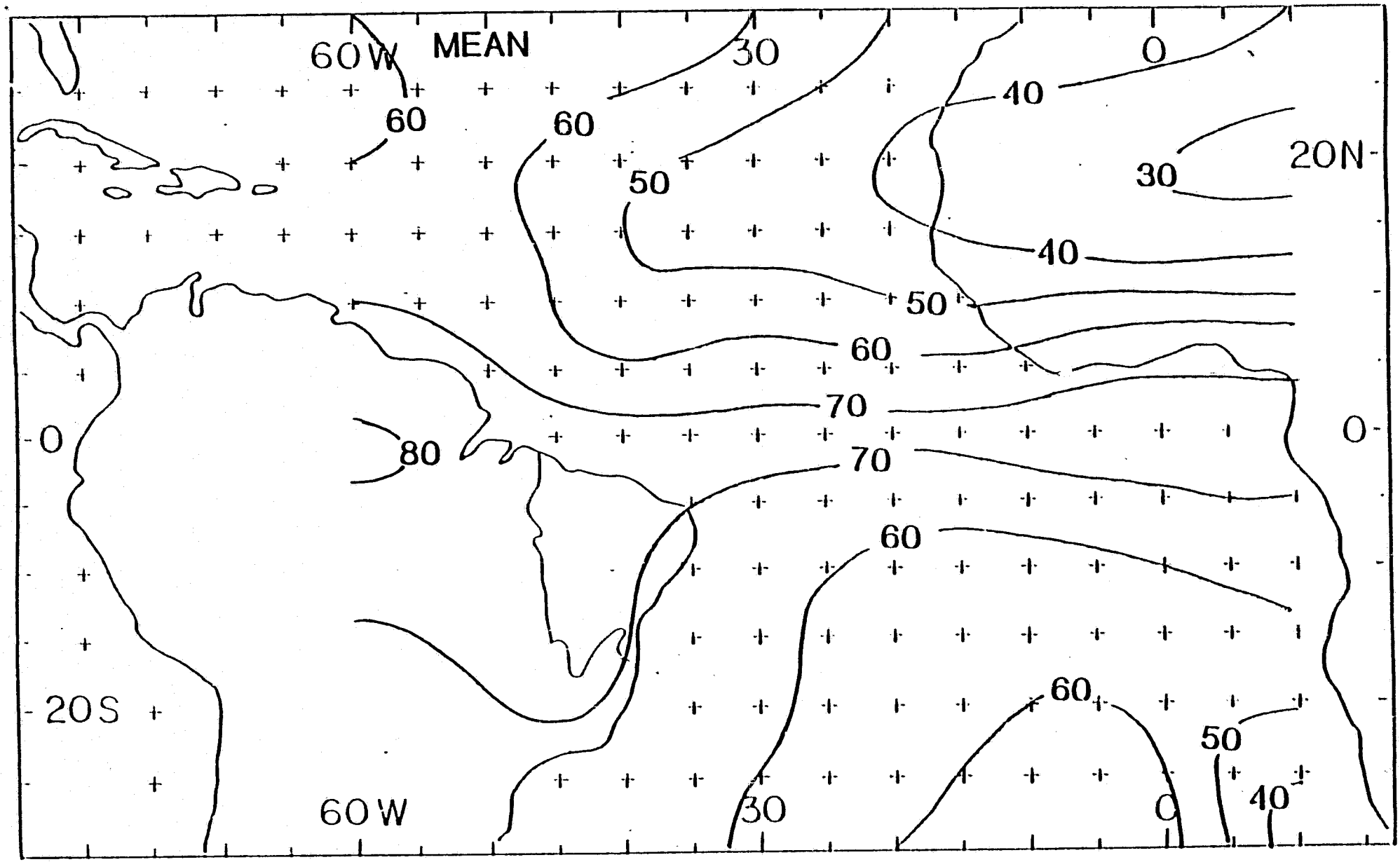
MEAN
60W
30
0
40
60
60
20N
30
50
40
50
60
70
0
80
0
70
60
20S
60
50
40
60W
30
0

Fig. 6.

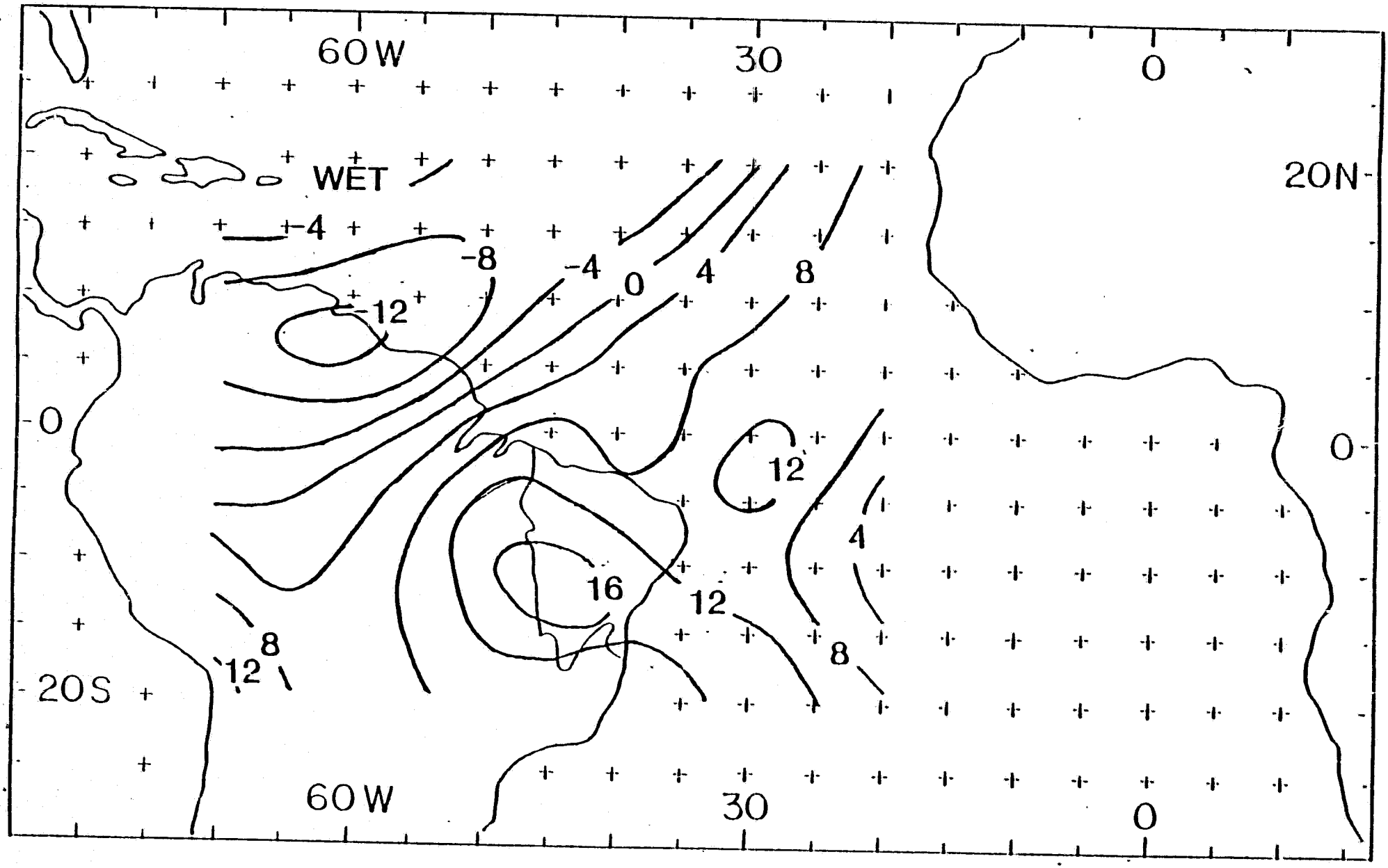

Fig. 7

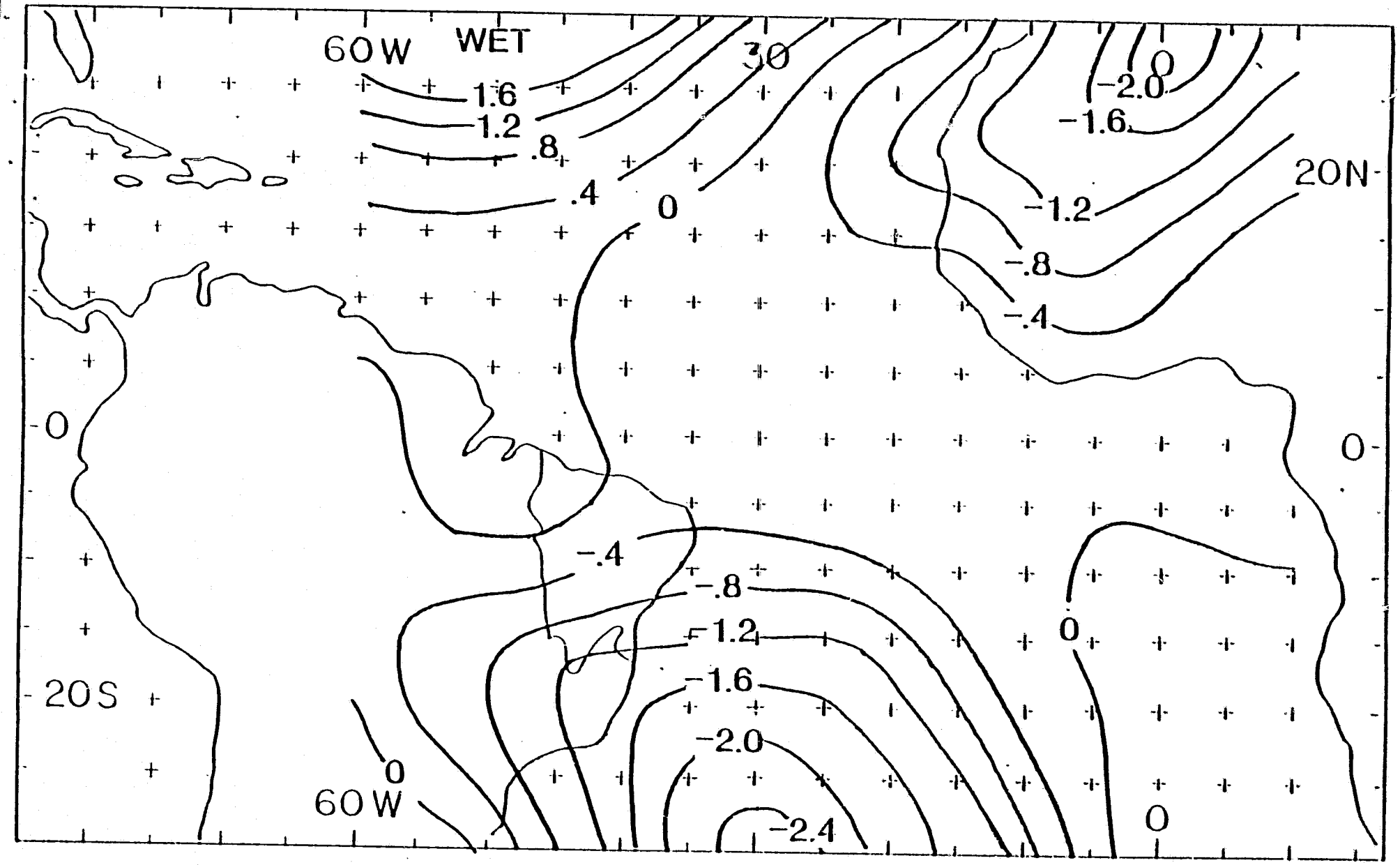

Fig. 8

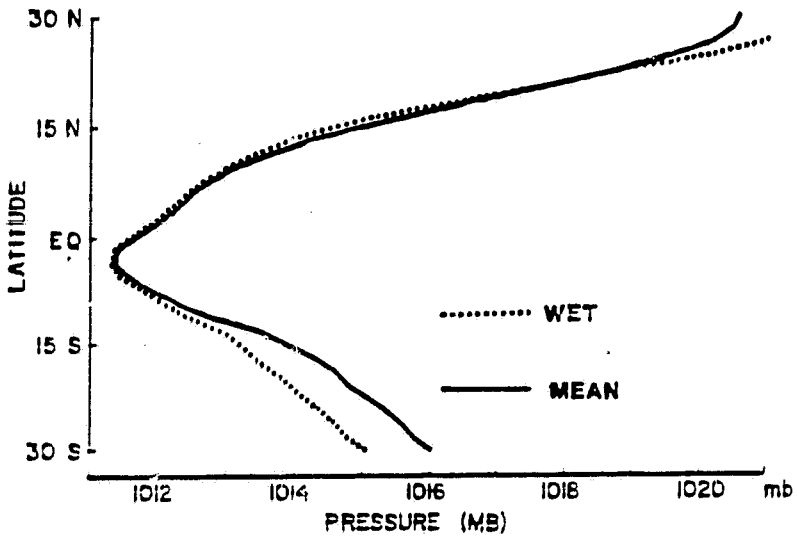

Fig. 9.

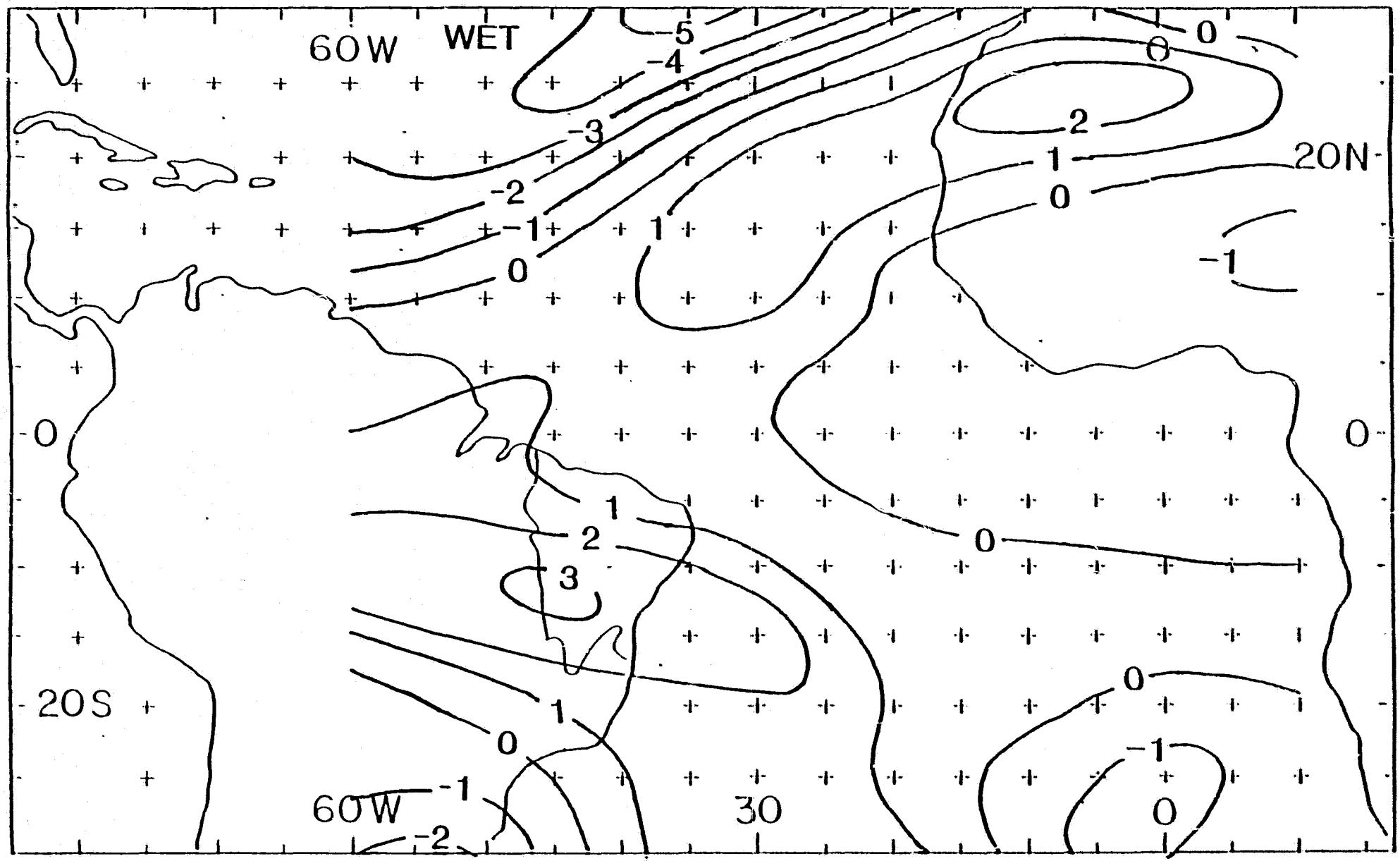

Fig. 10

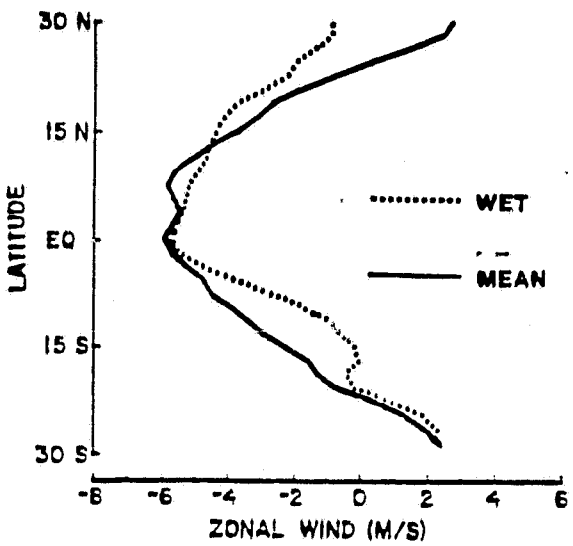

Fig. 11

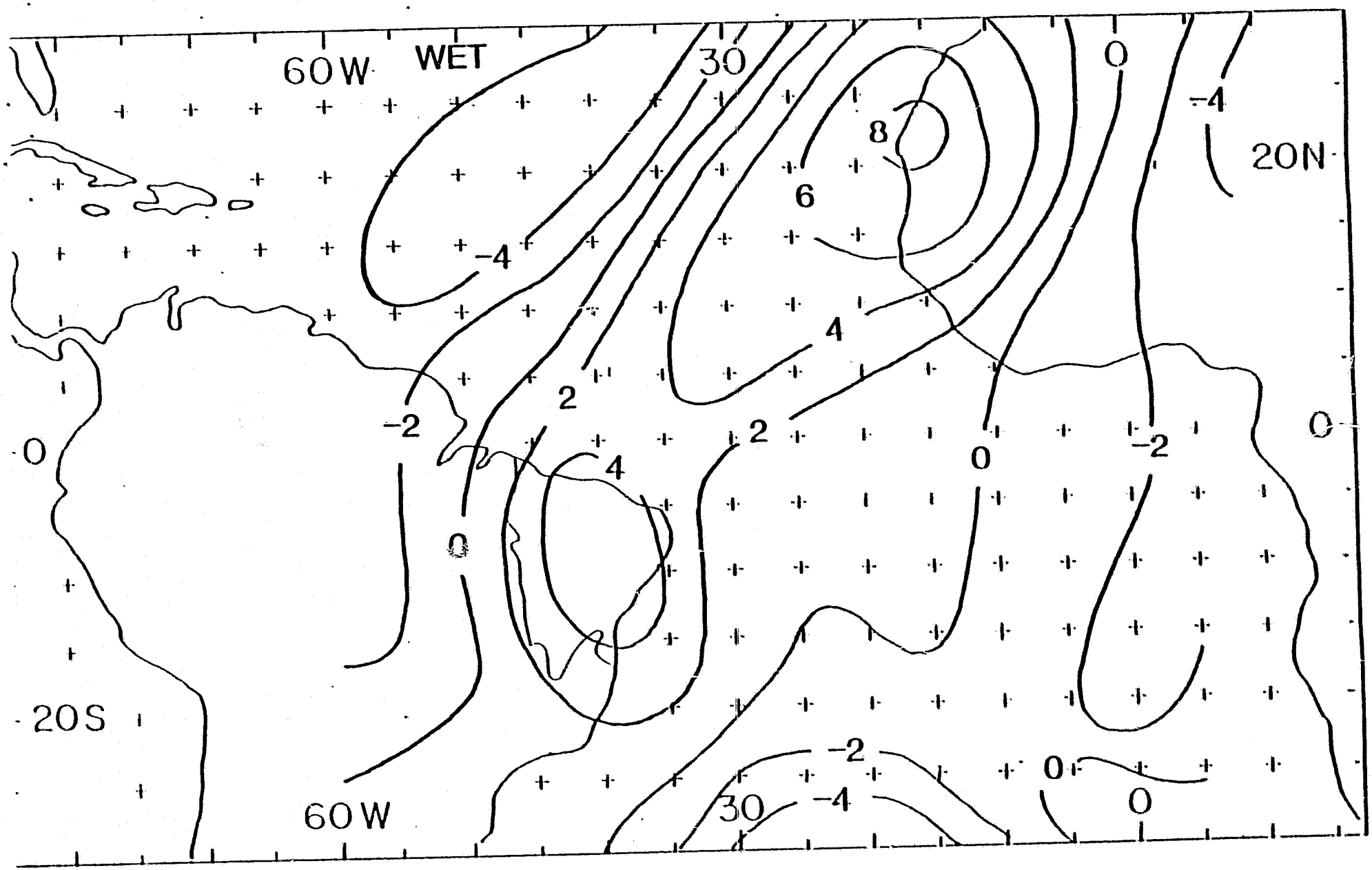

Fig 12

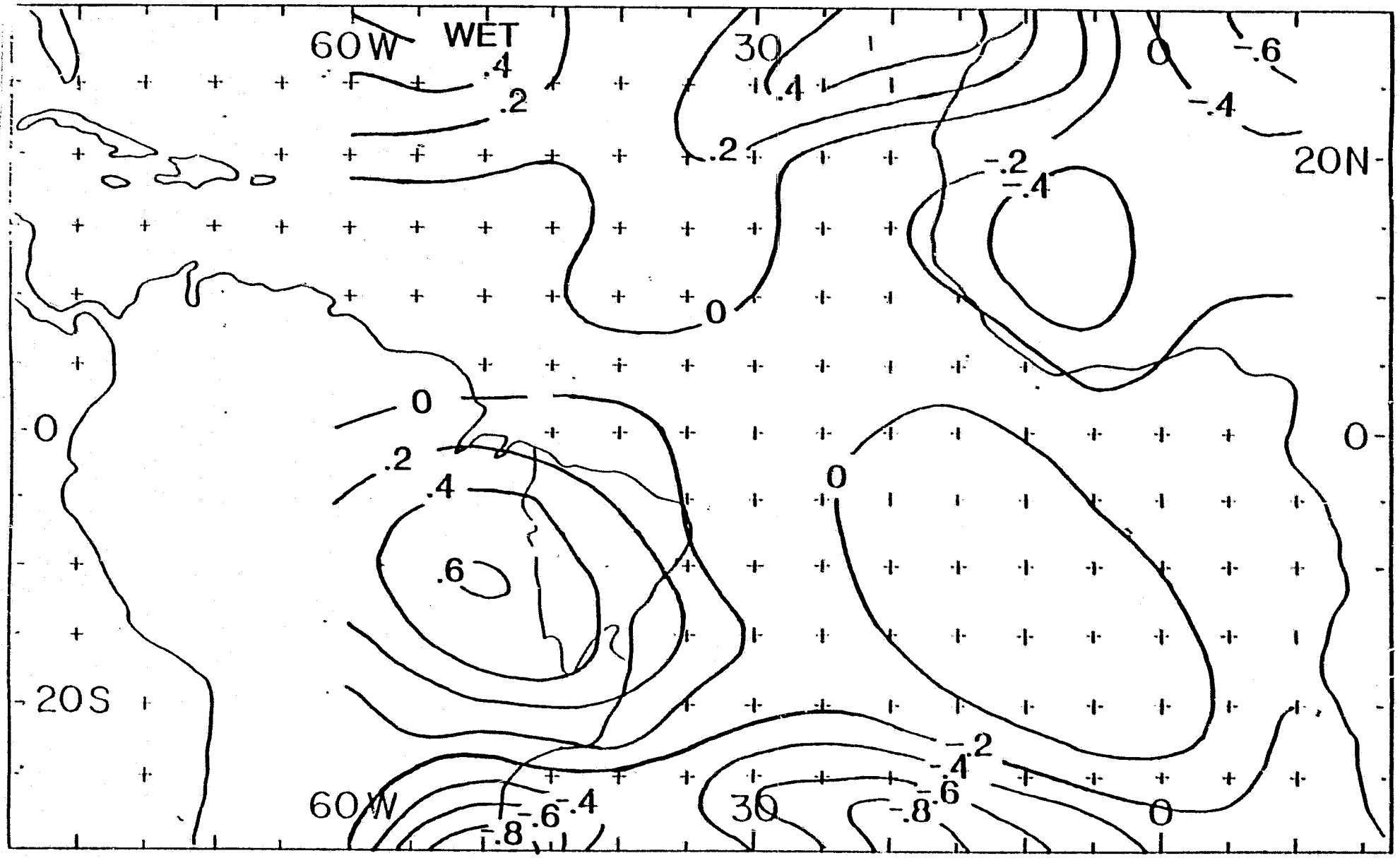

Fig. 13

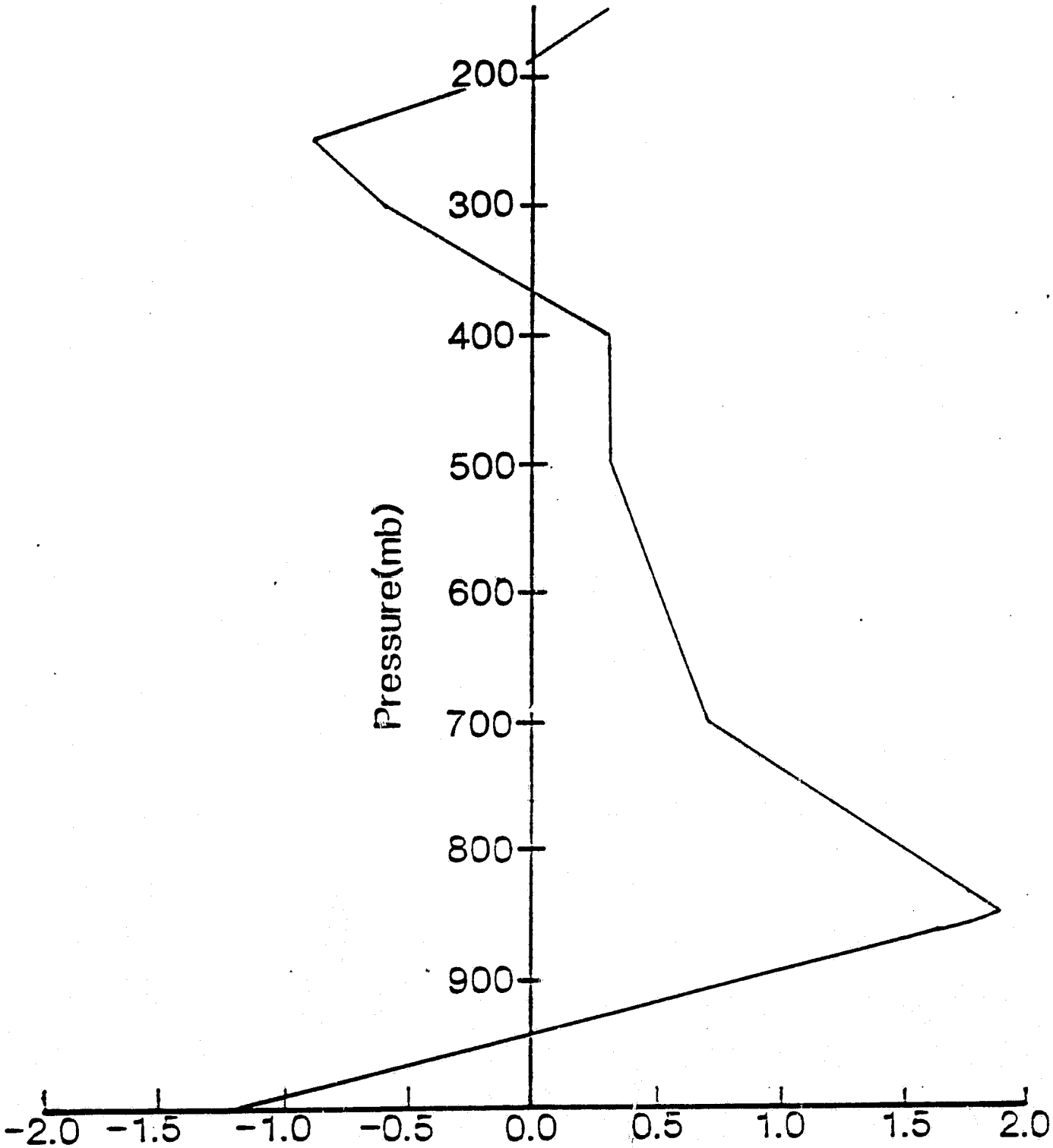
200
300
400
500
600
700
800
900
Pressure(mb)
-2.0
-1.5
-1.0
-0.5
0.0
0.5
1.0
1.5
2.0
Velocity Divergence

Fig. 14.

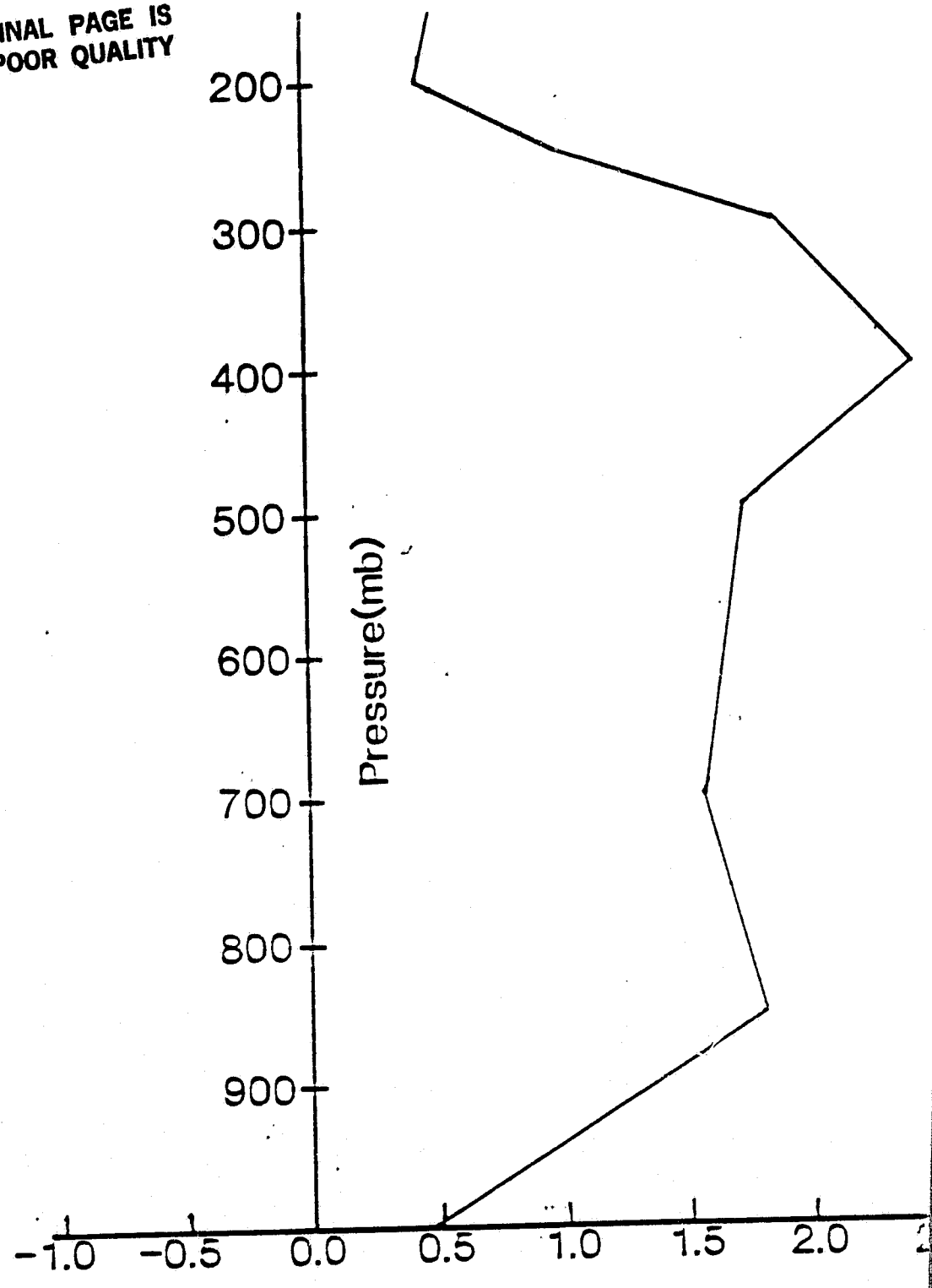

Zonal Wind
Departures

Fig. 15

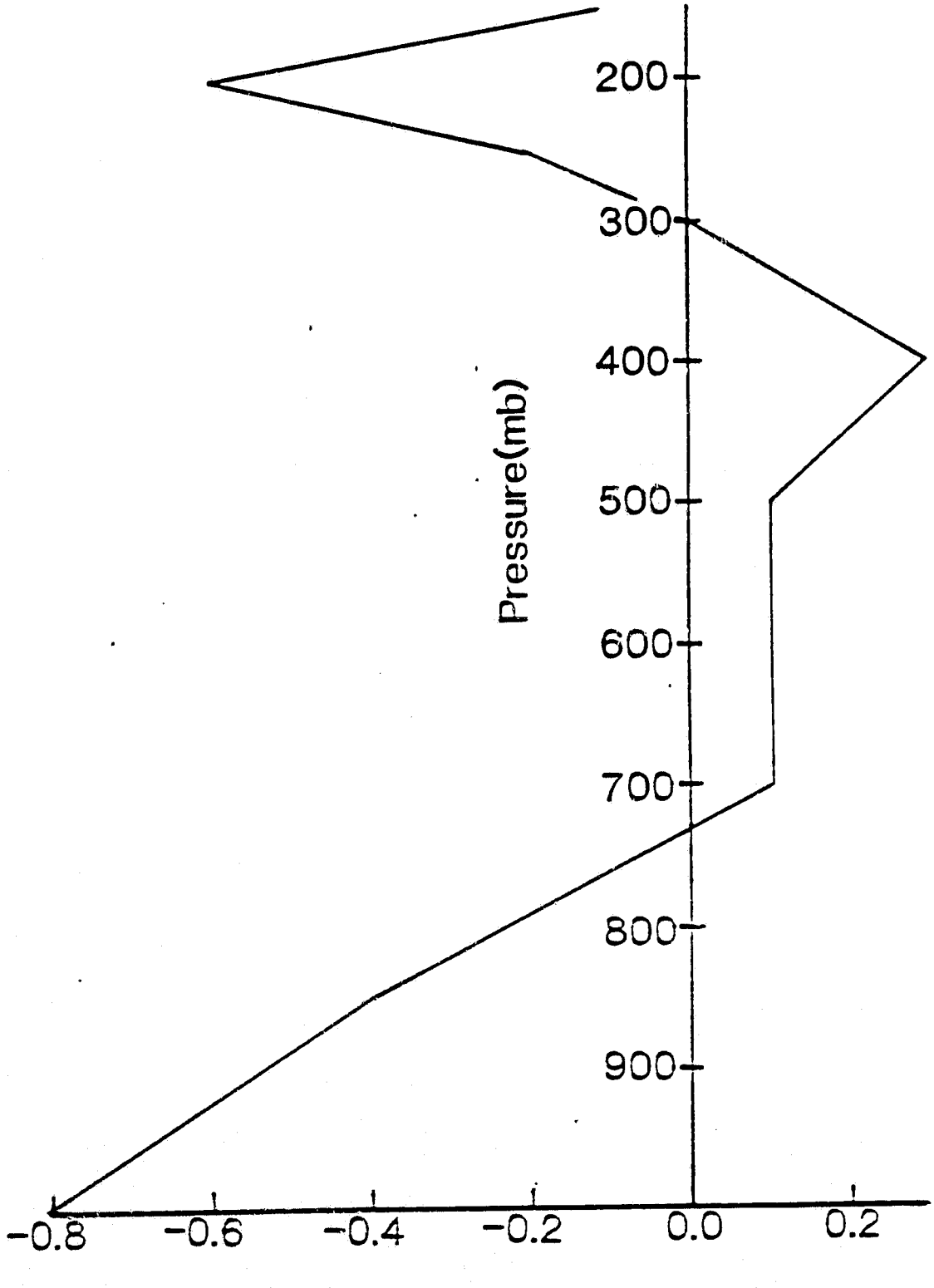

Velocity Divergence
Departures

Fig. 16.

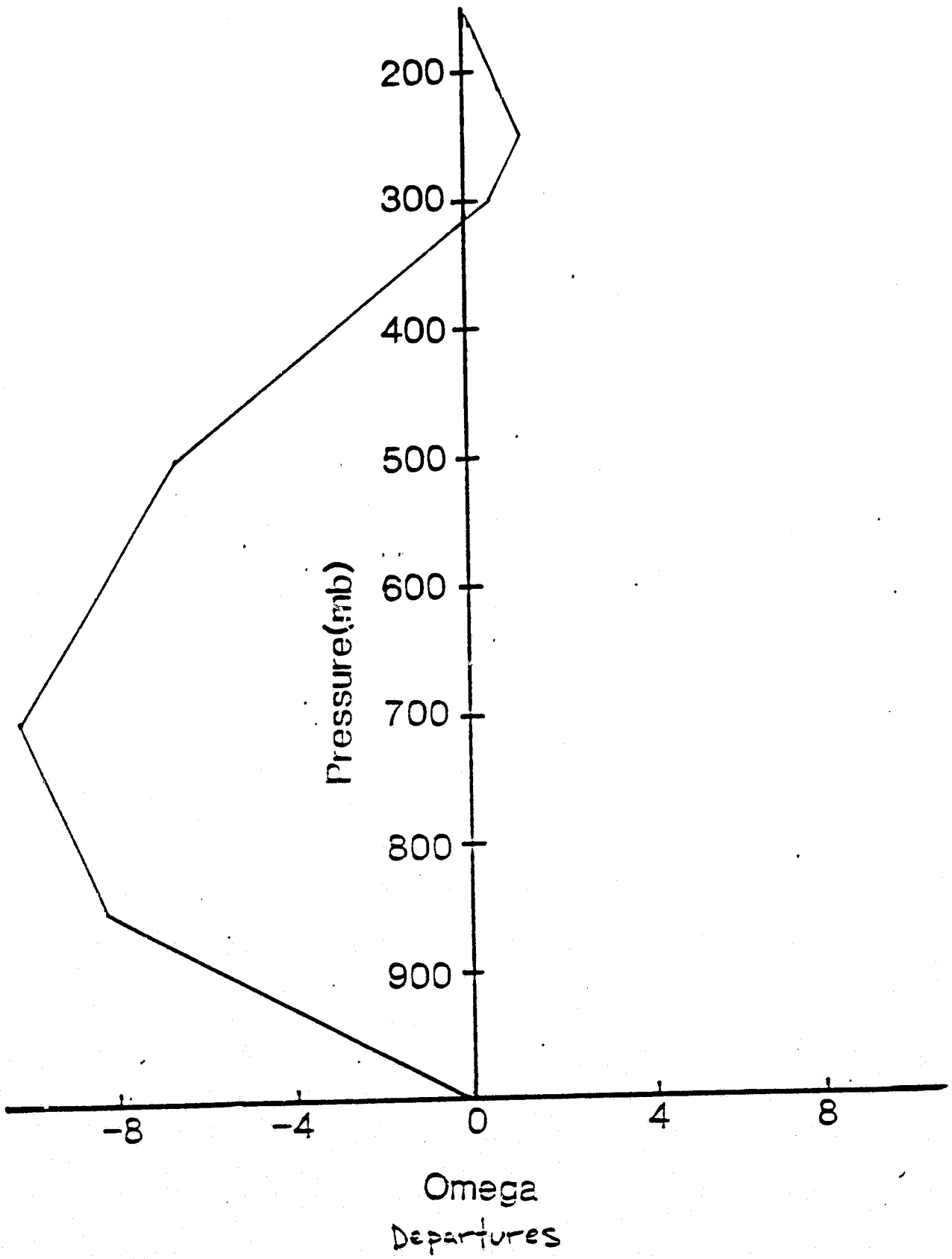
200
300
400
500
600
700
800
900
Pressure(mb)
-8
-4
0
4
8
Omega
Departures

Fig 17

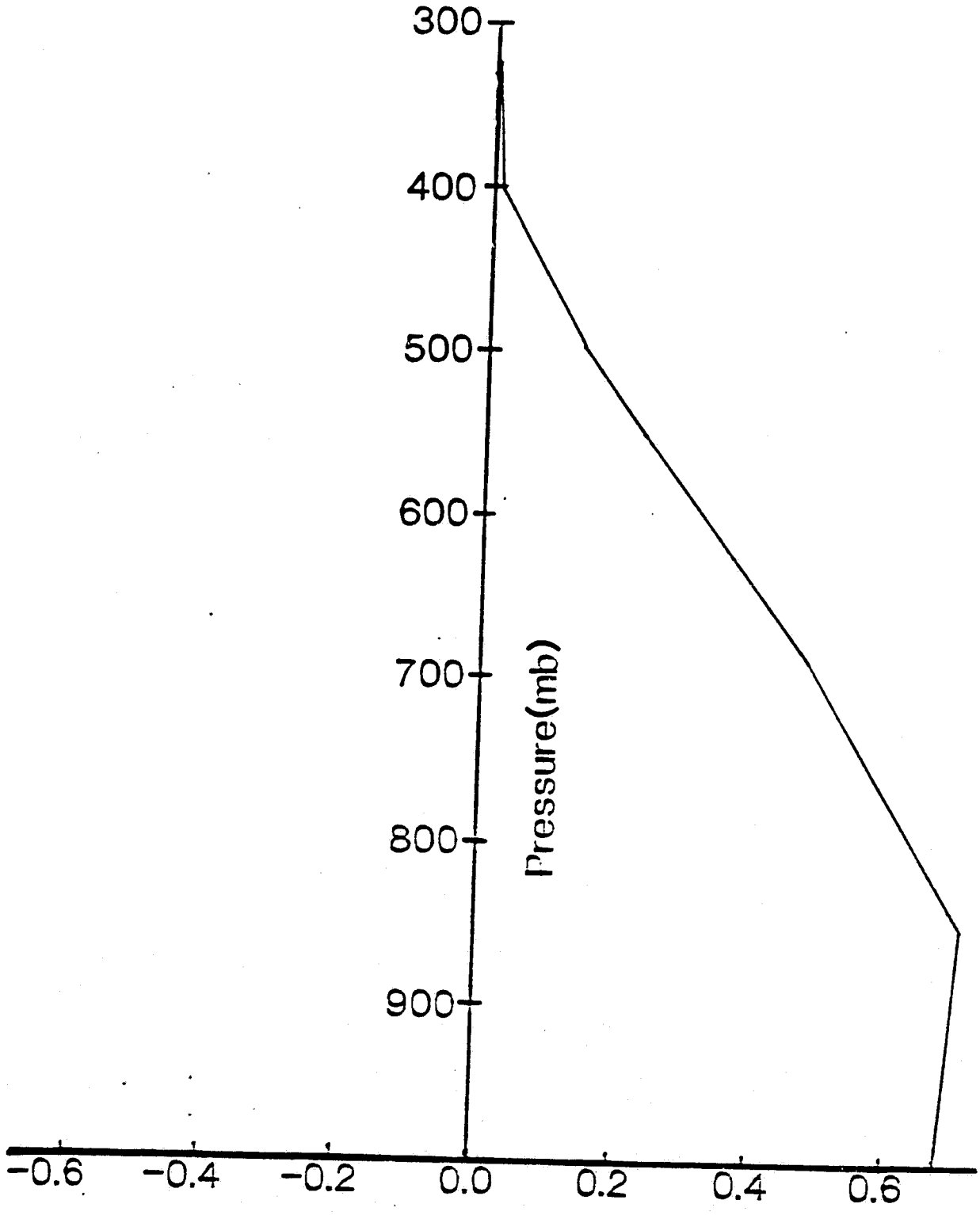

Mixing Ratio
Departures

Fig. 18

J. B. Elsner
Original draft.
Sent to Tellus
6 Sept. 1985

Daily Variability of Rainfall and Atmospheric Energetics Over Northeast Brazil During the Rainy Season of 1979

Dhirendra N. Sikdar and James B. Elsner

Atmospheric Sciences Division

Dept. of Geological/Geophysical Sciences

University of Wisconsin-Milwaukee

Milwaukee, WI 53211

USA

September 1985

Abstract

As an extension to recent studies concerning interannual and seasonal variability of rainfall over northeast Brazil, this study looks at the atmosphere immediately over northeast Brazil. Daily variability of rainfall, horizontal winds and thermodynamic energies are examined for the wet season (February through May) of 1979. A trend is observed in the temporal rainfall pattern, from short duration showers in the early season to longer and more vigorous systems in the later season. May is noted as a transitional month between the wet and dry seasons. Findings for dry days include: stronger low-level easterlies, a net export of moist energy and a composite upper-tropospheric cyclone centered over Salvador Brazil. Wet days are marked by comparatively large values of latent heat. It is concluded that regional subsidence plays a dominant role in modulating daily precipitation.

Introduction

If the interior of northeast Brazil, commonly known as the sertao, had a "true" desert climate, it would most likely be sparsely populated and sociological and economical hardships would be nominal. However, the climate of the sertao is problematic. Sufficient rains will occur for several consecutive years, arriving principally during the months of February through May, when crops and gardens flourish. Then, during other years, rain is extremely scarce and crops do not grow. Drought conditions may continue for prolonged periods; the drought of the 1950's is the most infamous example. The problem is compounded because the region is highly populated and survival depends on adequate rainfall. Coastal regions of northeast Brazil receive in the neighborhood of 2000 mm of rain annually and are exempt from radical variability experienced in the sertao.

Recently, there have been a number of studies concerning the climate variability of this region. Much of the work has been in the area of interannual rainfall variability as related to large-scale circulation patterns. To depict mechanisms of rainfall fluctuation, the departure patterns of SLP, wind and SST over the tropical Atlantic were investigated for composites of extremely dry and extremely wet years (Hastenrath and Heller, 1977). Drought years were noted by a far northerly position of the equatorial trough, and by the anomalously warm water in the North Atlantic and cold water south of the equator. During wet years, departure patterns were reversed.

Moura and Shukla (1981) conducted an experiment with the GLAS General Circulation Model, using a sea surface temperature anomaly pattern similiar to that found by Hastenrath and Heller. They concluded that the occurance of a warm anomaly in the North Atlantic and cold anomaly in the South Atlantic is conducive to a thermally direct meridional circulation, resulting in subsidence

and reduced rainfall over northeast Brazil.

Marques et. al., (1983) studied the interannual and seasonal variations in the atmosphere immediately over northeast Brazil. They found that the vertical structure of moist static energy during wet periods was similar to the structure in the equatorial trough. They also showed that during wet periods the lower-tropospheric easterlies were comparatively weak, indicating the proximity of the equatorial trough to the region. From this it was suggested that rainfall variations in northeast Brazil are not of local origin but appear to be connected with variations of the tropical general circulation.

As a natural extension to these studies, this work investigates the atmosphere over northeast Brazil on a daily basis. We studied daily rainfall, as well as the structure and energetics of the atmosphere, during the rainy season of 1979, with an emphasis on variations between wet and dry days. Specifically, we used a rainfall index on daily rainfall data, and following Marques, et. al. (1983) we developed a cylindrical grid whose base covers most of northeast Brazil. The grid was used in computation of energy and water vapor fluxes.

2. Region and Data Sources

We used a cylinder covering most of northeast Brazil, with 16 aerological stations within or immediately outside the circular base (Fig. 1). The cylinder was chosen to facilitate comparisons with interannual and seasonal variability and to aid in the flux computations. The cylinder base encloses the annual minimum-precipitation region (shown as the shaded area in Fig. 1) for the period 1931-1960 as computed by Strang (1972) and as appeared in Ramos (1975). The hatched area receives on the average less than 500 mm of rain per year, most of which occurs during February through May. The major hydrological concern of

the region, however, is not the annual mean but rather the variability of the yearly rainfall. The area of the base circle is approximately 1.5×10^6 km^2 and the height extends up to 100 mb.

The main data base consisting of 16 aerological stations was obtained from the National Climatic Data Center in Asheville North Carolina. Data were available for each station either at both 0000 and 1200 GMT or just 1200 GMT for February through May 1979. Components include geopotential heights, pressures, air temperature, relative humidity and the speed and direction of the wind at mandatory and significant levels. Data were composited at each station after a manual inspection for erroneous values. Compositing was done at 1000, 850, 700, 500, 400, 300, 250, 200, 150 and 100 mb levels. Composite profiles were lightly smoothed by removing the data value which exhibited the largest variance. Geopotential heights were computed from temperatures profile and compared with observed composite values. Only minor differences were noted, hence the observed values are used. Potential temperature lapse rates were found to be stable.

As a supplement to the aerological information, we used FGGE-level IIIb data grids for the area over Brazil and the tropical Atlantic sector from 30°N to 30°S. The primary element of interest from these data is zonal wind. Grid spacing is 1.875° lat-long, and vertical levels include mandatory levels up to 150 mb inclusive.

For the purpose of analysis and compositing, rainfall data were obtained from the superintendencia de Desenvolvimento do Nordeste in Recife, Pernambuco Brazil. Data include daily totals for the entire year of 1979 from more than a thousand stations in northeast Brazil. Twenty-one stations were chosen in the "dry region" (hatched region of Fig. 1) for use in this study. Elevations of stations ranged from 190 meters at Caico, Rio Grande do Norte to 770 meters at

Teixeira, Paraiba. Rainfall station locations are shown in Fig. 2, along with the mean annual isohyets computed by Strang (1972).

3. Rainfall Analysis

The rainy season over much of northeast Brazil consists primarily of the months February through May and occurs in conjunction with the southern most latitudinal extension of the equatorial trough, although even during these months the trough remains north of the region. Precipitation in the region, similar to much of the tropics, occurs in showers; therefore, when analyzing rainfall it is better to use a small network of rainfall stations rather than a single station (Riehl, 1979). In the present study, we compute normalized departures of rainfall using a network of stations in the "dry region." A list of the rainfall stations used in the indexing appears in Table 1. The method of computing departures is outlined in Kraus (1977) and provides a useful index of regional rainfall for each day. The purpose of creating a rainfall index is two-fold. First, it aids in the time-series analysis of data. Secondly, it is used to help determine days of extreme rainfall for compositing the upper-air information.

We briefly describe the method. Let r_{ij} be the daily rainfall of station i during day j, J be the number of days in the analysis period, and J_i be the number of days with a record at station i during the period J. Also, let I be the number of stations in the region to be analyzed and I_j the number of regional stations in operation on day j. Thus, the mean daily rainfall at station i and its variance are:

$$\bar{r}_i = \frac{1}{J_i} \sum_j r_{ij} , \qquad \sigma_i = \left(\frac{1}{J_i} \sum_j r_{ij}^2 - \bar{r}_i^2 \right)^{\frac{1}{2}}$$

The normalization is $x_{ij} = (r_{ij} - \bar{r}_i)/\sigma_i$ and the area-averaged value of x_{ij}

for the day j is $a_j = \frac{1}{I_j} \sum_i x_{ij}$. We must first check to see if spatial variations of the x_{ij}'s between different places within the region are small relative to day-to-day variations as a whole (a_j's). To do this we use the F-test or ratio-of-variance test.

Let v_t be the variance in time and v_a be the variance in space. Then $v_t = \frac{\sum I_j a_j^2}{J-1}$ and $v_a = \frac{N - \sum I_j a_j^2}{N-J}$ where $N = \sum I_j = \sum J_i = 2428$ in this study. For our data then:

Variances:	$v_t = 2.71$	$v_a = 0.91$
Degrees of freedom:	$J-1 = 119$	$N-J = 2308$

The ratio of variance (v_t / v_a) estimate is 2.97 which is significant, since the limiting value of F for 1 percent probability is 1.32. In other words, the probability that the differences between days in the combined regional rainfall record is a result of random fluctuations is less than 1:100.

Table 2 shows both the area-averaged normalized rainfall anomalies (a_j) and the unnormalized area averages ($\overline{x}_j$). From the table we can see that May was the driest, of the four months, particularly toward the end of the month. May had nine days without any recorded precipitation, while February, March and April combined had a total of ten days without rainfall. This finding along with earlier studies establishing the wet season as February through April, leads us to conclude that May is a transition month between the winter dry season and summer wet season. Analysis of the concentration of precipitation reveals the following: 14 percent of the days with rain during the rainy season account for 51 percent of the rainfall (Fig. 3), while 31 percent of the days account for 76 percent. Conversely, precipitation from 50 percent of the days with the least rain amounts to only 8 percent of the total. For compositing

purposes we chose the 19 days with no precipitation as the dry composite. Then, for similarity, we picked 19 days with the largest area-averaged normalized precipitation for the wet composite.

Since we have shown that area-averaged normalized rainfall departures are not random in time, we employ time-series techniques as a way to further understand physical processes which produce the precipitation. Figure 4 shows graphs of raw and five-day smoothed normalized departures. Outstanding peaks are noted at the end of March and again at the end of April. May is conspicuous for a tapering of positive rainfall departures, indicating a transition from the wet to dry season. A closer look at the time-series of raw departures reveals that daily variability during February is large compared with the remainder of the rainy season. This indicates a possible a trend from short duration showers in the early season to more intense and persistent rainfall systems in the later season. Figure 5 shows the correlogram and smoothed-power spectrum of raw normalized rainfall departures. From the autocorrelation we see a sharp drop in positive correlation for the first several lags, indicating little persistence beyond 2 or 3 days. The power spectrum reveals significant peaks (above the 90 percent level) at 8 and 13 days. Speculation as to the physical causes for these apparent oscillations is given later.

In the sections which follow, wet and dry composites of variables refer to the average of these variables over 19 of the wettest days and over 19 of the driest days, respectively, during the rainy season of 1979.

4. Horizontal Wind

Vertical cross-sections of zonal wind and meridional wind components were plotted for both wet and dry composites. Data are from the FGGE-level IIIb grids. Analyses were subjected to a 25-point smoothing filter. The

cross-section of zonal wind is shown in Figs. 6 a and b. The cross-section is along the 41°15′ meridian, which slices the cylinder approximately in two equal halves.

One of the most striking differences between composites is the relative strength of low- and mid-level easterlies during dry days. This finding is nearly identical to findings from studies of interannual and seasonal variations in the structure of the zonal wind (Hastenrath and Heller (1977), Marques et. al. (1983), etc.). Riehl (1979) remarked about the lack of a wind discontinuity at the trade wind inversion base. Strong easterlies during dry days at low levels suggest strong trade-wind subsidence at middle and high levels over the region. In other words, we imply relatively strong sinking anticyclonic (counterclockwise) diverging air over northeast Brazil and the western South Atlantic. This air originates from upper-level cyclonic vortices. The existence of these vortices near northeast Brazil has been documented by Kousky and Gan (1981). High-level cyclonic rotation can be inferred from the meridional wind component. Figures 7 a and b show a vertical cross-section of meridional wind along the latitude circle 7°30′S. Clearly shown during dry days is a gradient of meridional wind from west to east at upper levels, which suggests a cyclonic rotation. The gradient is markedly weaker during wet days. A plot of upper-tropospheric horizontal wind vectors averaged over three vertical levels (150, 200, 250 mbs) is shown in Figs. 8 a and b. Clearly depicted is the cyclonic vortex over northeast Brazil during dry days. The vortex is absent during wet days. In the realm of speculation, the 8- and 13-day peaks in the power spectrum of rainfall may be related to the cycle of upper-level vortices.

Lag-cross correlations were computed between rainfall departures and relative vorticity. Upper-level cyclonic vorticity was negatively correlated

with rainfall, particularly around minus one lag, as was expected. Positive correlations appear around minus seven lag. Coefficients are near 0.55. Low-level anticyclonic vorticity showed no large correlations with rainfall.

Another interesting difference in the zonal wind cross-sections is the strength of westerlies north of 10°N. During wet days we see a gradual increase in westerlies moving north from 10°N while during dry days westerlies increase rapidly over the same region. We also note a southward shift of the zone of low-level easterlies from wet days to dry days, indicating increasing northeasterly trades between 12° and 20°N and a slackening of the southeast trades near 10°S during wet days. Riehl (1979) has noted that the subtropical ridge slopes equatorward much more on the winter-hemisphere side of the equatorial trough than on the summer side. We have found in the northern hemisphere that the slope of the subtropical ridge (indicated by the slope of the line separating higher-latitude westerlies from lower-latitude easterlies) is greater during wet days as compared with dry days. These differences suggest a possible connection of northern hemisphere mid-latitude synoptic patterns on rainfall over northeast Brazil.

5. Thermodynamic Energy Content of the Cylinder

The horizontal surfaces of the cylinder are divided into a grid with 9 points equally spaced around the perimeter and one center grid point. The diameter of the cylinder is approximately 1400 km. Distance between points on the perimeter is nearly 500 km. The cylinder is slightly larger than the one used by Marques, et. al., (1983). The vertical is divided into nine levels with an equal separation of 100 mb from 1000 to 100 mb. Vertical-space sections were constructed and analyzed for each parameter, with pressure on a linear scale as the ordinate, and the circumference distance as the abscissae. Grid values were

picked up at each grid point for all levels. Thermodynamic energy components were then computed before averaging horizontally to yield the mean values around the cylinder for each level. Layer averaged values were used in the discussion. Energy values were also computed for the centered grid.

Tables 3 a,b,c and d display the values of energy content for the atmosphere over northeast Brazil during wet and dry days, and for the center grid for both composites. For both wet and dry composites, we see a minimum in total thermodynamic energy in the middle troposphere (Fig. 9). According to Riehl (1979), this is typical of the tropical atmosphere.

From vertical profiles of moist static energy, some interesting observations can be made. In the lowest layer, total energies are the same for wet and dry composites. Wet days have more latent heat but less sensible heat, while dry days have more sensible heat but less latent heat. Between 400 and 900 mb, the effect of greater latent heat offsets the sensible heat, resulting in large total energies during wet days. Between 200 and 400 mb, the latent energy vanishes and the effect of sensible heat dominates, producing larger total energy values during dry days. Further, between 100 and 200 mb, sensible heat is strongest during wet days, resulting in larger total energy in the upper troposphere. These profiles are similar to Marques et. al., (1983) for wet and dry years, but the values we obtained are slightly smaller at all levels. Possible explanations for these profile observations include, stronger mid-tropospheric subsidence warming during dry days, indicating the proximity of the South Atlantic high (SAH). Stronger undiluted cumulonimbus transports lower tropospheric heat to the upper layers during wet days. And stronger cumulus transports latent heat to low and middle tropospheres during wet days.

For the center grid we find large differences in total energy between composites, with wet days having significantly more total energy than dry days

particularly in the middle troposphere (Fig. 10). We also note that the minimum energy layer during wet days is the 500-600 mb layer, while for dry days it is the 600-700 mb layer. These results suggest more extensive cumulus transport during wet days.

6. Normal Component of Velocity

Figure 11 shows the mass adjusted normal velocity for both wet and dry composites. Adjustment requirements are small, particularly for wet days. Velocities are also small, as can be expected from the scale of our cylinder. Positive values indicate inward convergence. During wet days we note low-level convergence and upper-level divergence but in the mid-troposphere we find a region of convergence overlaying a region of divergence. Dry days show nearly a reversal in this structure. Again, these findings are similar to findings of Marques et. al. (1983) for interannual and seasonal variations. For dry days, relative convergence at upper and middle levels imply broad-scale subsidence over northeast Brazil. Whereas for wet days low-level relative convergence produces broad-scale ascent.

Mass adjusted wind divergence in each layer of the cylinder was estimated using the formula, $D = (S/A)V_n$, where S is the circumference of the cylinder, A is the area and V_n is the mass-adjusted normal velocity component. Vertical motions were then computed using the kinematic method. Wet days have a composite mass-adjusted upward motion throughout the troposphere, with dry days showing sinking motions. Figures 12 a and b show a composite of percent bright (cold) cloud amount for wet and dry days. As expected, large-scale descending motions of the dry days over Nordeste agree well with the low percentage of bright cloudiness in the region. We note that during wet days the intertropical cloud band has a considerably larger meridional extent. These two distinct

vertical mass couplings support our findings in regard to the vertical cross sections of zonal and meridional wind discussed in Section 4. During dry days, subsidence is stronger, inhibiting the development of cumulonimbus clouds and therefore, rainfall.

7. Heat and Moisture Fluxes

Sensible and latent heat fluxes have been evaluated at each boundary grid and for the cylinder as a whole. The equations used were developed in Marques et. al. (1983) and are shown here for convenience.

$$SHF = \frac{R}{g}\int_{p_t}^{p_o}(C_pT + \phi)\,V_n\,dp \quad \text{and} \quad LHF = \frac{R}{g}\int_{p_t}^{p_o} Lq\,V_n\,dp \quad \text{where}$$

dp: is the vertical layer = 100 mb

V_n: is the normal component of horizontal valocity in ms^{-1}

$C_pT + \phi$: is the sensible heat in $KJkg^{-1}$

R: is the radius of the cylinder ~700 km

g: is gravity = 9.8 ms^{-2}

Lq: is the latent heat in $KJkg^{-1}$

For the cylinder as a whole, these equations are integrated along the boundary. Flux values are also computed at each boundary grid.

Table 4 shows fluxes of $(C_pT + \phi)$, Lq and $(C_pt + \phi + Lq)$ for both composites. During wet days we find inward flux of sensible heat in low layers below 600 mb with a net export above. In contrast, during dry days we find a net export below 600 mb with a net import above. Strongest fluxes of sensible heat are found during wet days at upper levels. The export above 600 mb during these days amounts to 11.9×10^{13} Js^{-1}. Fluxes of water vapor are comparatively

weak. However, we find low-level inward moisture flux below 600 mb during wet days amounting to 1.6×10^{15} Js^{-1}, while during dry days there is a net export of 0.2×10^{13} Js^{-1}.

We divided the cylinder approximately in half from northeast to southwest and totaled the moisture flux across the northwest and southeast halves of the circumference. Results indicate a moisture flux into the cylinder from the northwest and a slightly weaker outflux of moisture from the southeast. Direction of flux is almost the same for both wet and dry composites, but, during wet days the region recieves approximately 17 percent more moist energy than during dry days.

8. Summary and Conclusions

Daily variability of rainfall, horizontal wind and thermodynamic energies over northeast Brazil have been examined for the rainy season of 1979. We have found that there are significant differences between wet and dry days over the region.

Rainfall was analyzed by indexing daily totals from stations in a specific "dry region" over a portion of northeast Brazil. We found that, in the region as a whole, daily fluctuations were not random. Applying time-series techniques to rainfall data we found significant peaks in the frequency domain at 8 and 13 days. We speculate that these peaks are related to propagation/formation of upper-level cyclonic vortices. We also found that May is a transition month between the well defined wet and dry seasons.

Vertical cross-sections of zonal wind reveal stronger low- and middle-level easterlies during dry days. Analysis of wind vectors averaged for three tropospheric levels indicate the existence of an upper tropospheric cyclonic vortex during dry days. Converging air at this level is forced to

descend and warm adiabatically, resulting in a strengthened trade wind inversion, which in turn inhibits precipitation. Because the findings show no wind discontinuity at the base or top of the inversion, we conclude that the low-level wind responds to increased subsidence through an increase in horizontal speed. Averaged normal velocities suggest low-level convergence and upper-level divergence during wet days. A reversal of this pattern was noted during dry days. Averaged speeds were small, as can be expected on this scale.

Comparatively large values of sensible heat in upper levels and larger latent heat in low and middle levels during wet days lead us to conclude that larger and/or more undiluted cumulonimbus clouds transport lower-tropospheric heat to upper layers and stronger cumulus transport latent heat to low and middle troposphères. Also we detected a low-level influx of moisture to the region during wet days, while a weak export of moisture at low levels is noted during dry days. The strongest inward-moist energy fluxes are found along the northwest half of the cylinder circumference for both wet and dry days. Possible moisture sources are the Amazon basin and the equatorial trough.

From analysis of results it appears that rainfall on a daily basis is closely related to the strength of subsidence over the region, which inhibits growth of cumulus and cumulonimbus transports. This in turn is controlled in part by the existence of upper-tropospheric cyclonic vortices. When a cyclonic vortex is situated near Salvador, subsidence is enhanced, creating a stronger inversion over northeast Brazil. It would be worthwhile to repeat this investigation for several years, including years of extreme drought and extreme rainfall.

Acknowledgements. The authers wish to thank Margaret Kleiber for typing the manuscript and Bill Lueders for editing. This work was supported by the Space

and Science Applications office, National Aeronautics and Space Administration under grant no. NAG 5-384. A partial support for graduate students and computer usage came from the UWM Graduate School.

References

Hastenrath, S., and L. Heller, 1977: Dynamics of climatic hazards in northeast Brazil. Quart. J. Roy. Meteor. Soc., 103, 77-92.

Kousky, V. E., and M. A. Gan, 1981: Upper tropospheric cyclonic vortices in the tropical South Atlantic. Tellus, 33, 538-551.

Kraus, E. B., 1977: Subtropical droughts and cross-equatorial energy transports. Mon. Wea. Rev., 105, 1009-1018.

Marques, V. S., B. Rao, and L. C. B. Molion, 1983: Inter-annual and seasonal variations in the structure and energetics of the atmosphere over NE Brazil. Tellus, 35A, 136-148.

Moura, A. D., and J. Shukla, 1981: On the dynamics of droughts in NE Brazil: Observations, theory and numerical experiments with a general circulation model. J. Atmos. Sci., 38, 2653-2675.

Ramos, R. P. L., 1975: Precipitation characteristics in northeast Brazil. J. Geophys. Res., 80, 1665-1678.

Riehl, H., 1979: Climate and weather in the tropics. Academic Press, New York.

Strang, D. M. D., 1972: Climatological analysis of rainfall normals in northeastern Brazil. Pap. IAE-M-02/72, 70 pp., Centro Tecnico Aerospacial, Sao Jose dos Campos, Brazil, 1972.

Figure Legends

Fig. 1 Regional map of northeast Brazil with sounding station locations and dry region shaded. Perimeter of the cylinder base depicted.

Fig. 2 Mean annual isohyets over northeast Brazil. Rainfall stations are marked by dots. Stations used in the rainfall indexing are numbered.

Fig. 3 Graph of cumulative percent total regional daily precipitation versus cumulative percent days.

Fig. 4 Graphs of raw and five day smoothed normalized rainfall departures for the period February through May of 1979.

Fig. 5 Correlogram and smoothed power spectrum of raw normalized rainfall departures.

Figs. 6 a and b Vertical cross sections of zonal wind along the longitude 41° 15′ W for wet and dry episodes.

Figs. 7 a and b Vertical cross sections of meridional wind along the latitude 7° 30′ S for wet and dry episodes.

Figs. 8 a and b Upper tropospheric horizontal wind vectors averaged over 150, 200 and 250 mb for wet and dry episodes. Length of vectors is proportional to speed.

Fig. 9 Vertical profiles of total static energies and dry static energies averaged around the perimeter for wet and dry episodes.

Fig. 10 Same as Fig. 9 except at center grid only.

Fig. 11 Vertical profiles of mass adjusted normal velocity for wet and dry episodes.

Figs. 12 a and b Analysis of composite percent bright (cold) cloud amount over the region for wet and dry episodes.

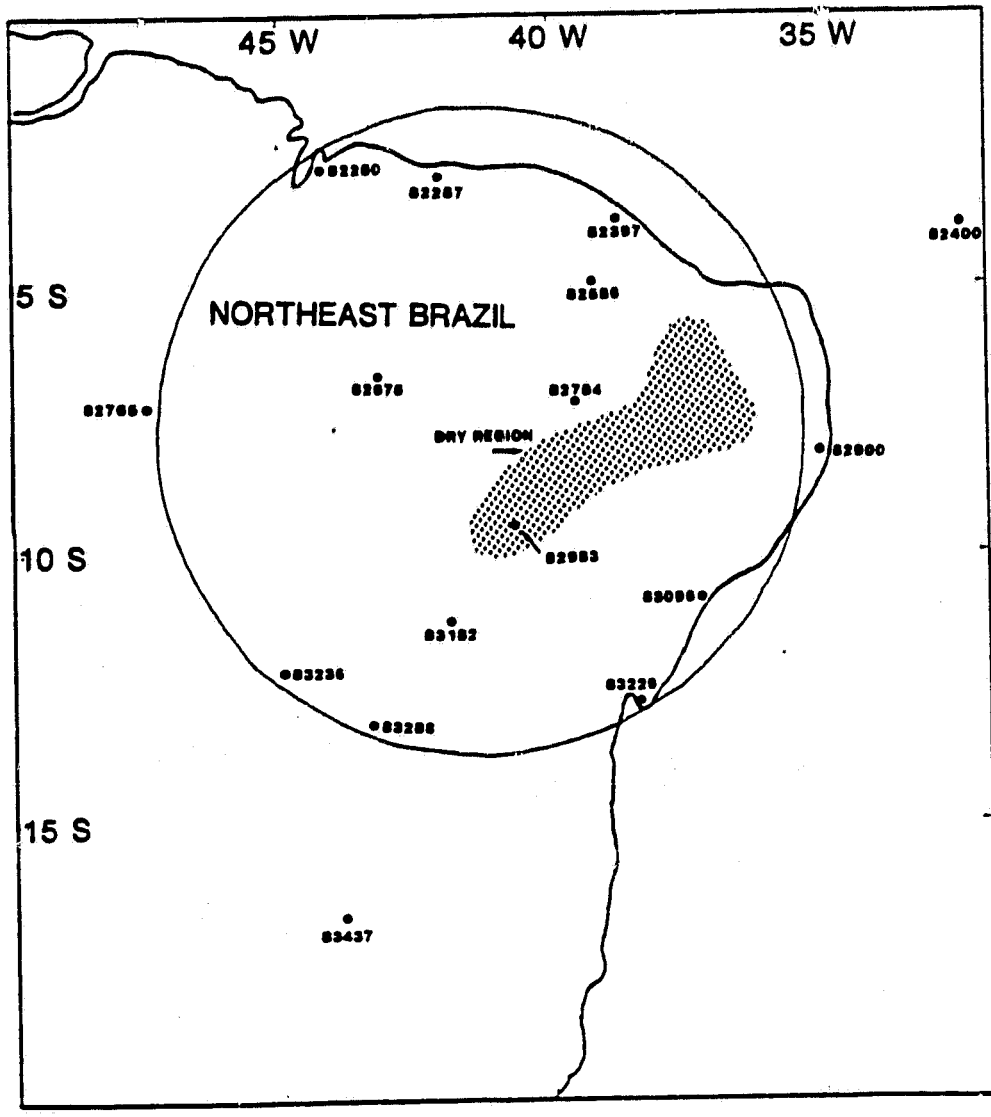

Fig. 1

Fig. 1

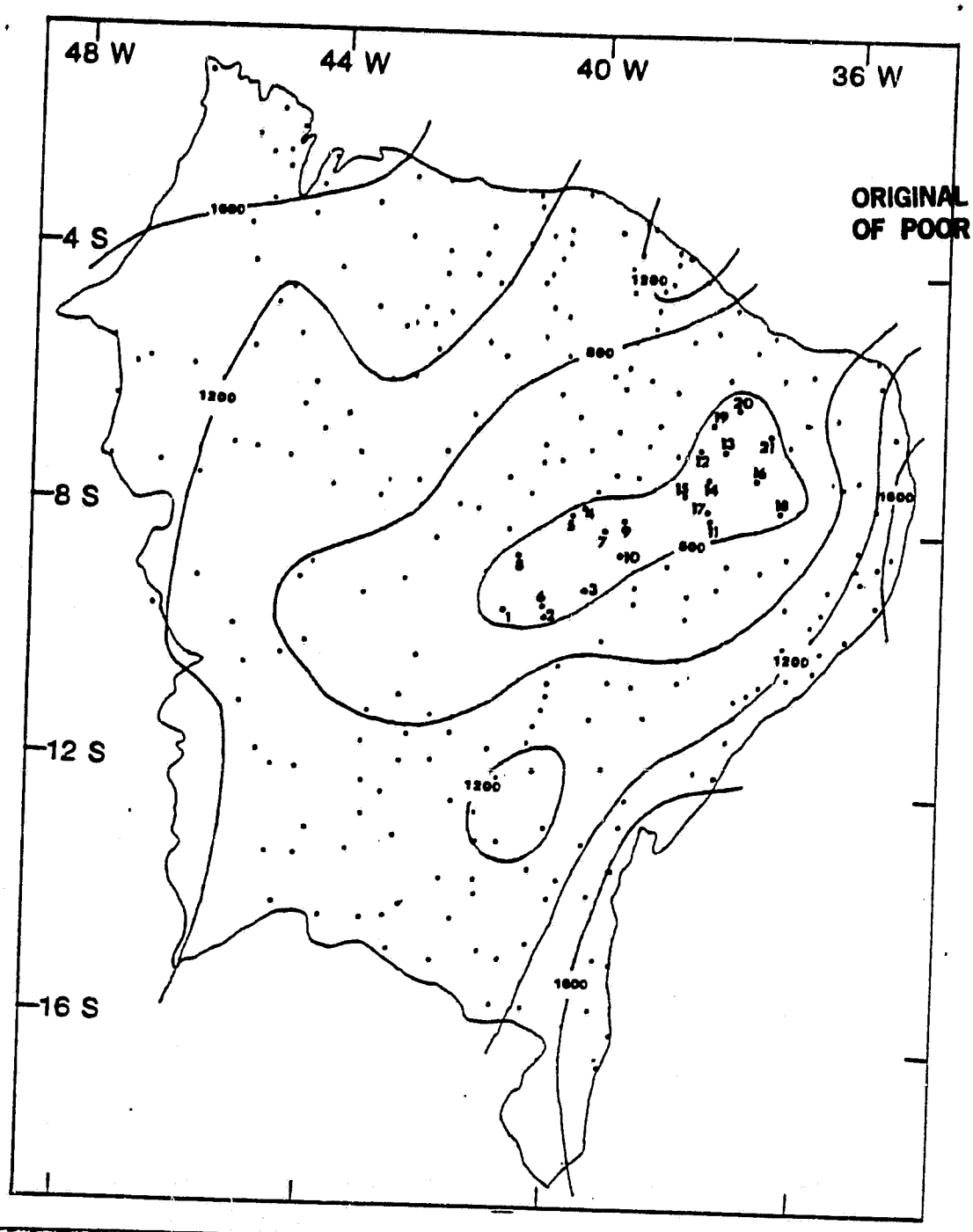

ORIGINAL PAGE IS
OF POOR QUALITY

Fig. 2

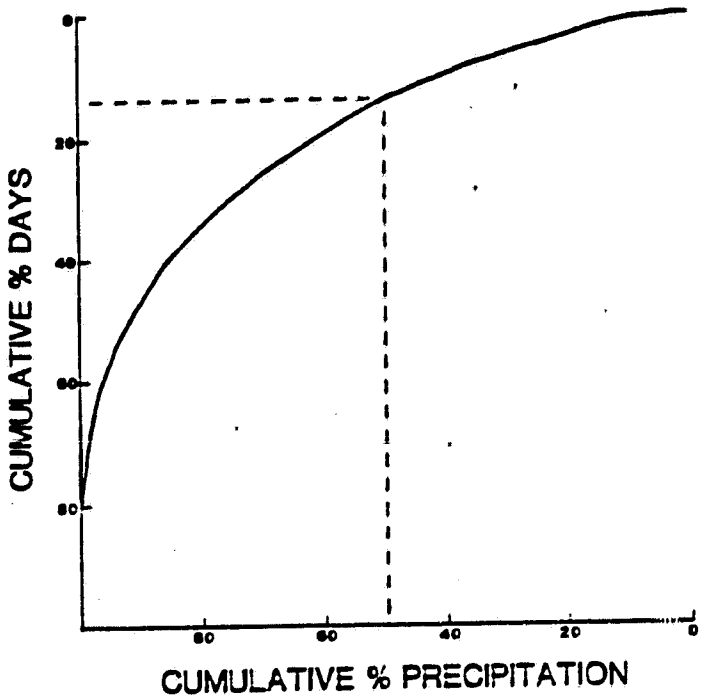

Fig. 3

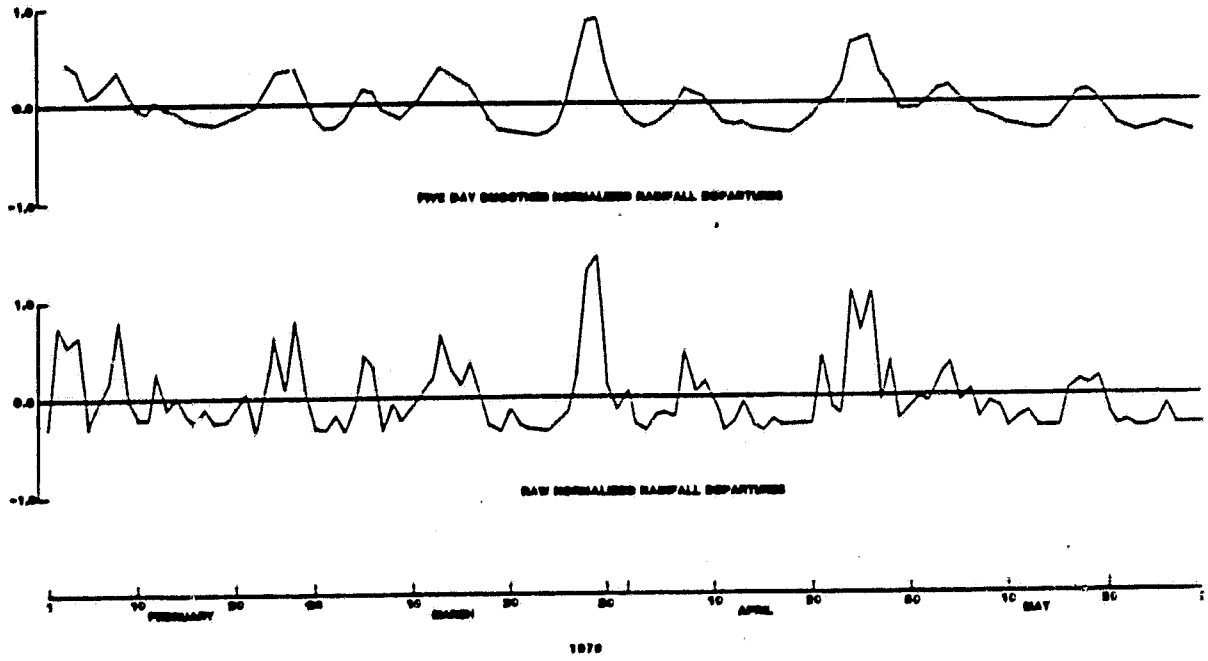

Fig. 4

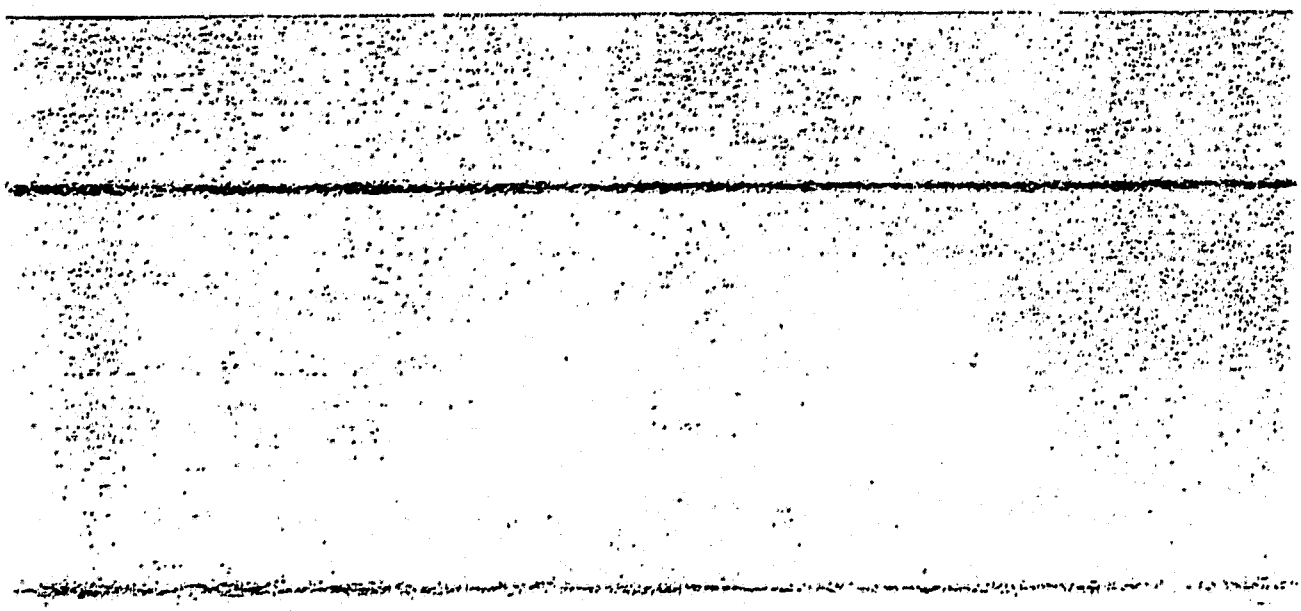

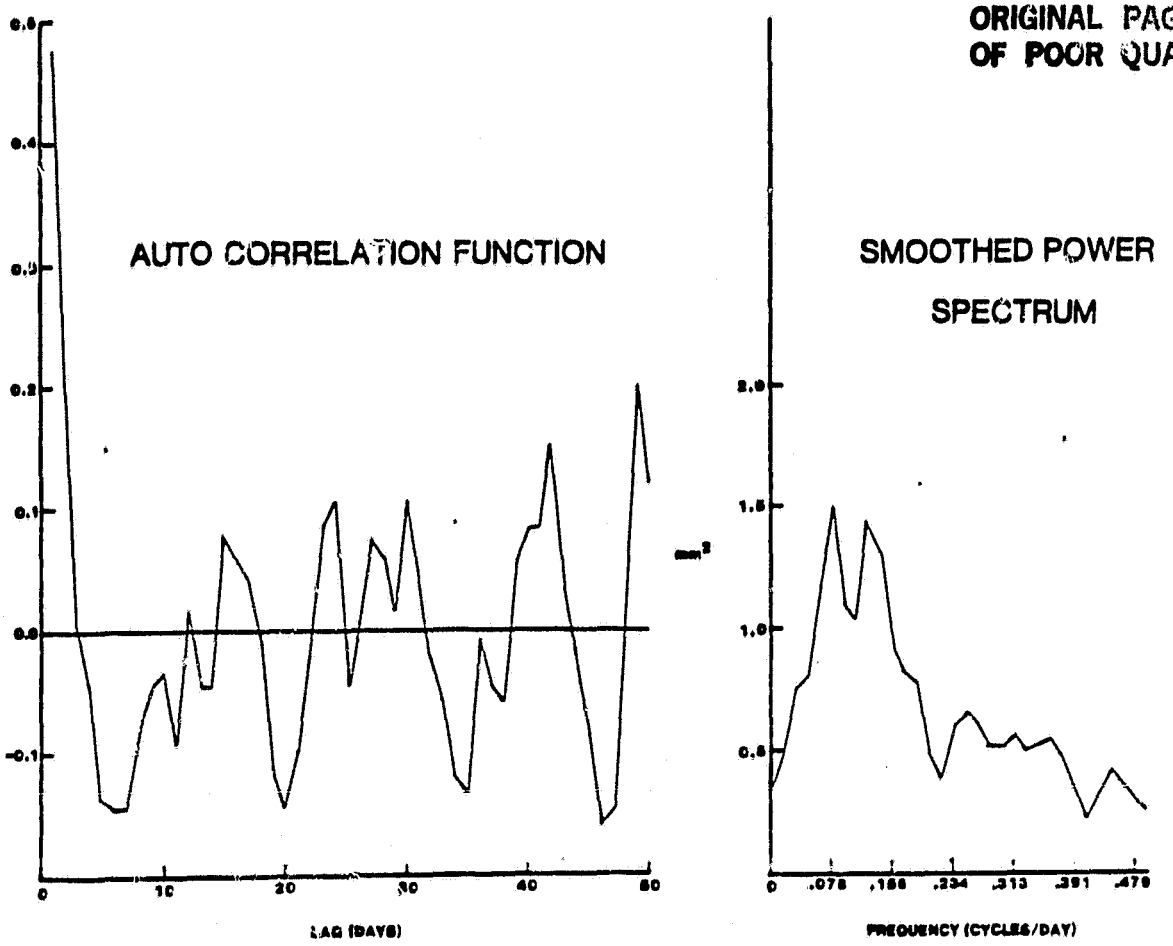

Fig 5

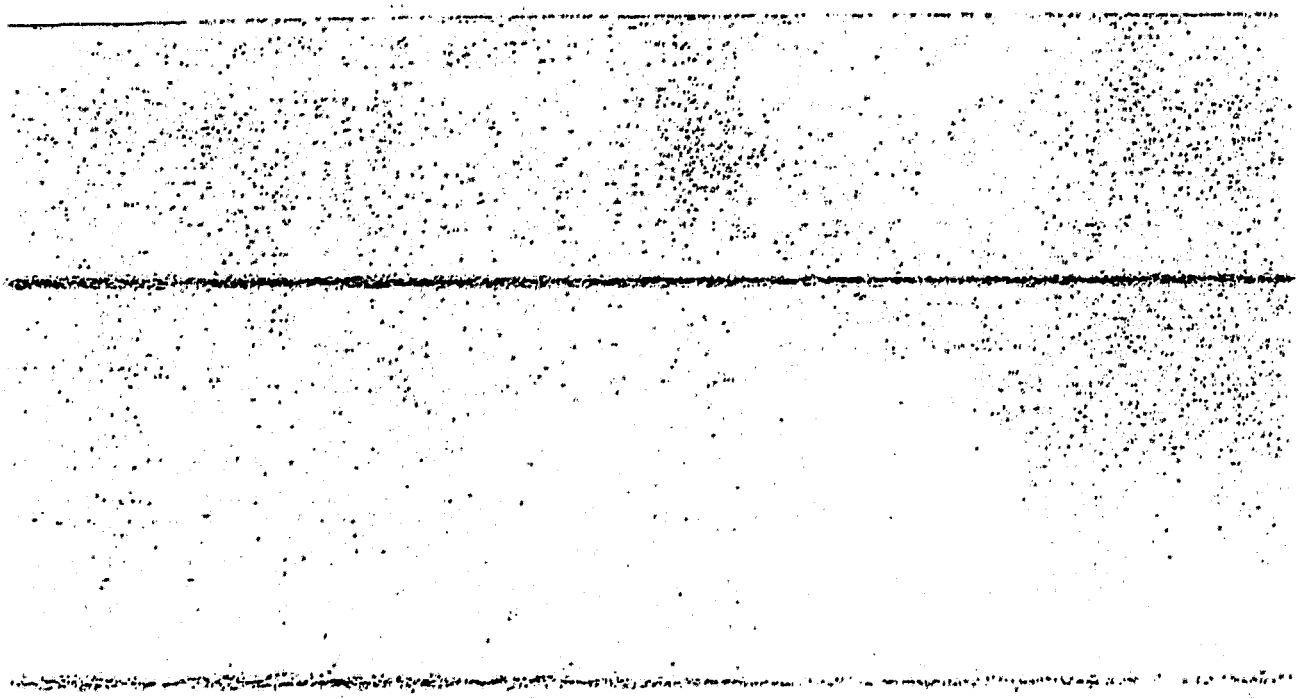

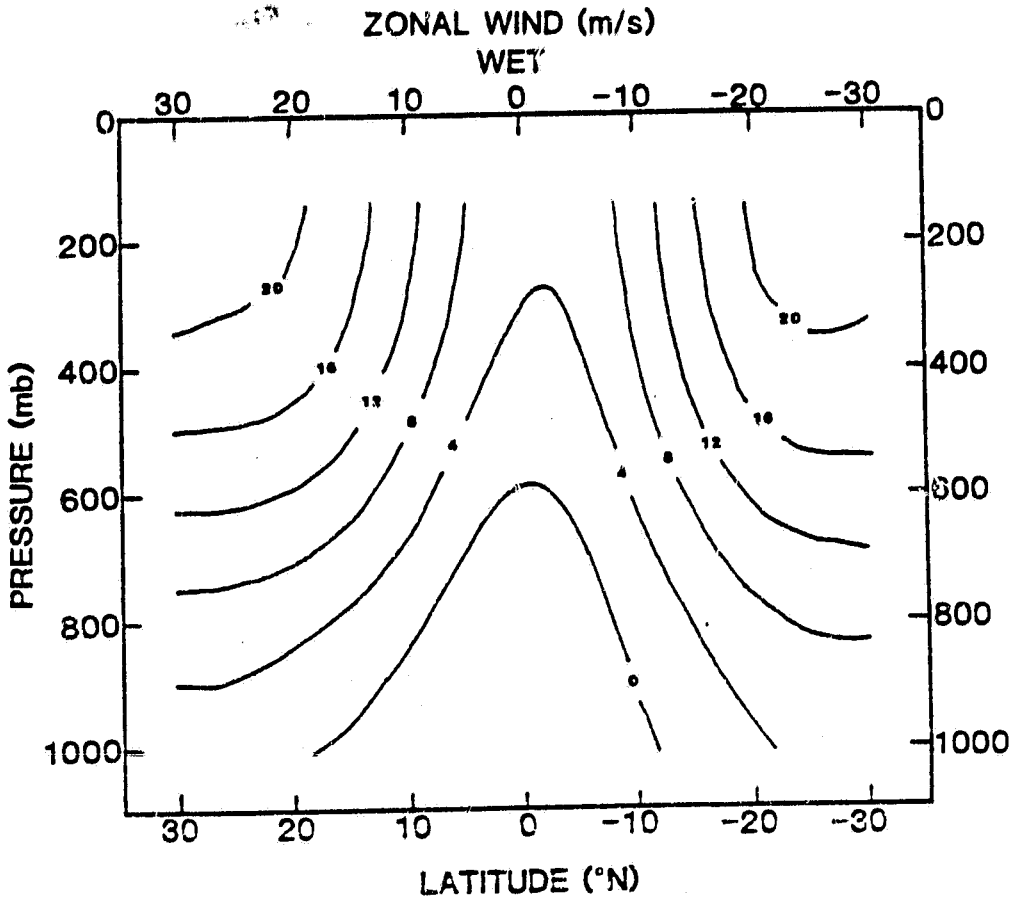
ZONAL WIND (m/s)
WET
30 20 10 0 -10 -20 -30
0
200
400
600
800
1000
PRESSURE (mb)
LATITUDE (°N)

Fig. 6a

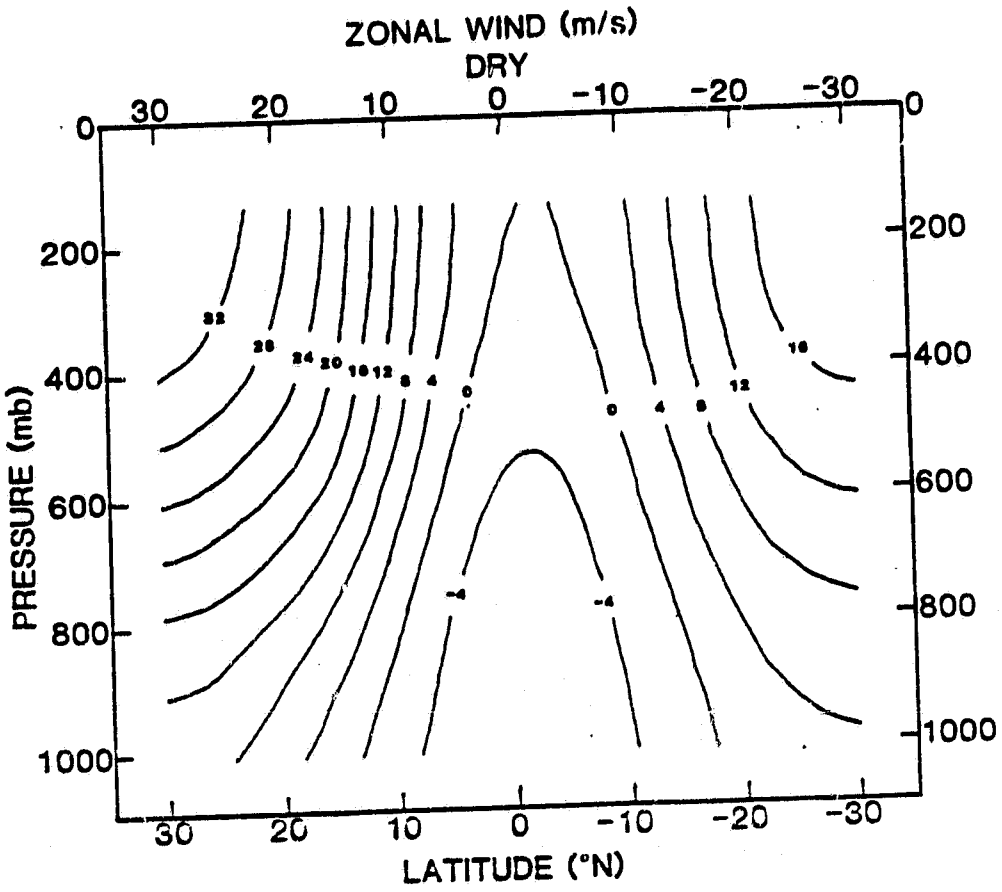
ZONAL WIND (m/s)
DRY
30 20 10 0 -10 -20 -30
0
200
400
600
800
1000
PRESSURE (mb)
LATITUDE (°N)
32
28
24
20
16
12
8
4
0
-4
-4
0
4
8
12
16

Fig. 6 b

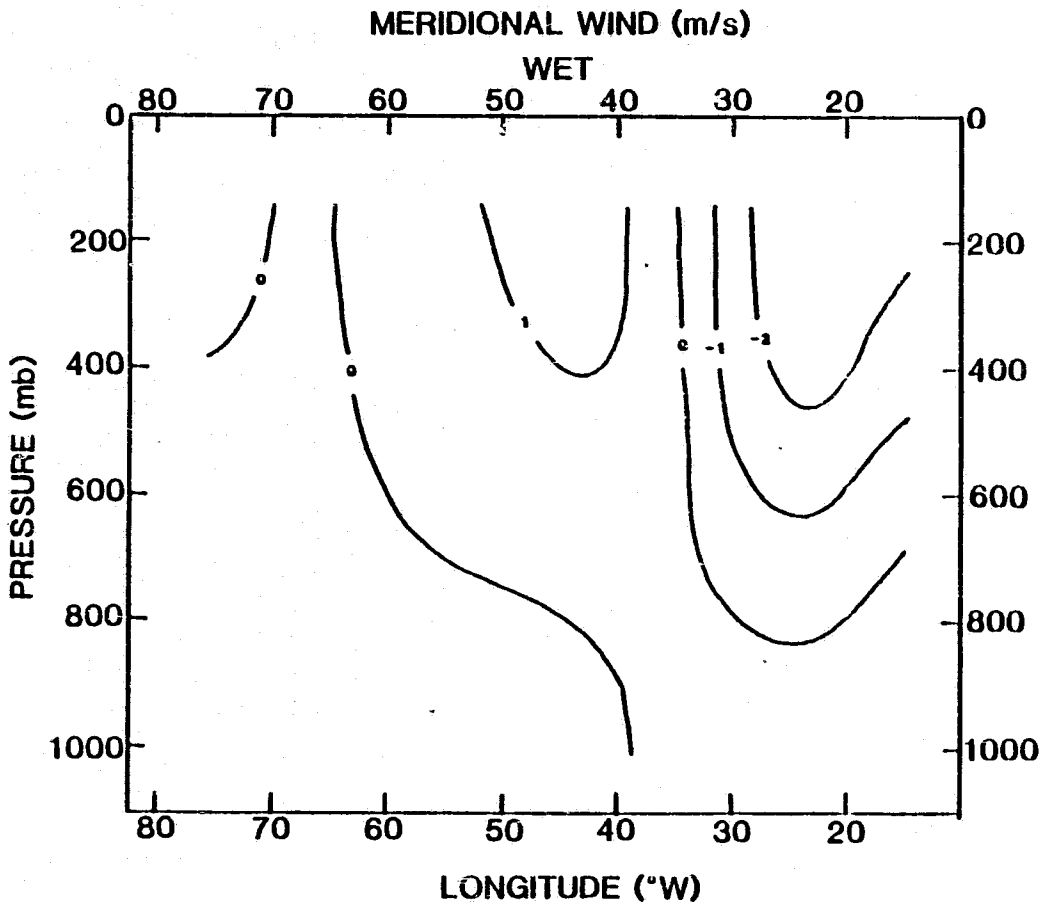
MERIDIONAL WIND (m/s)
WET
0
80
70
60
50
40
30
20
0
200
400
600
800
1000
PRESSURE (mb)
1
0
-1
-2
LONGITUDE (°W)

Fig. 7a

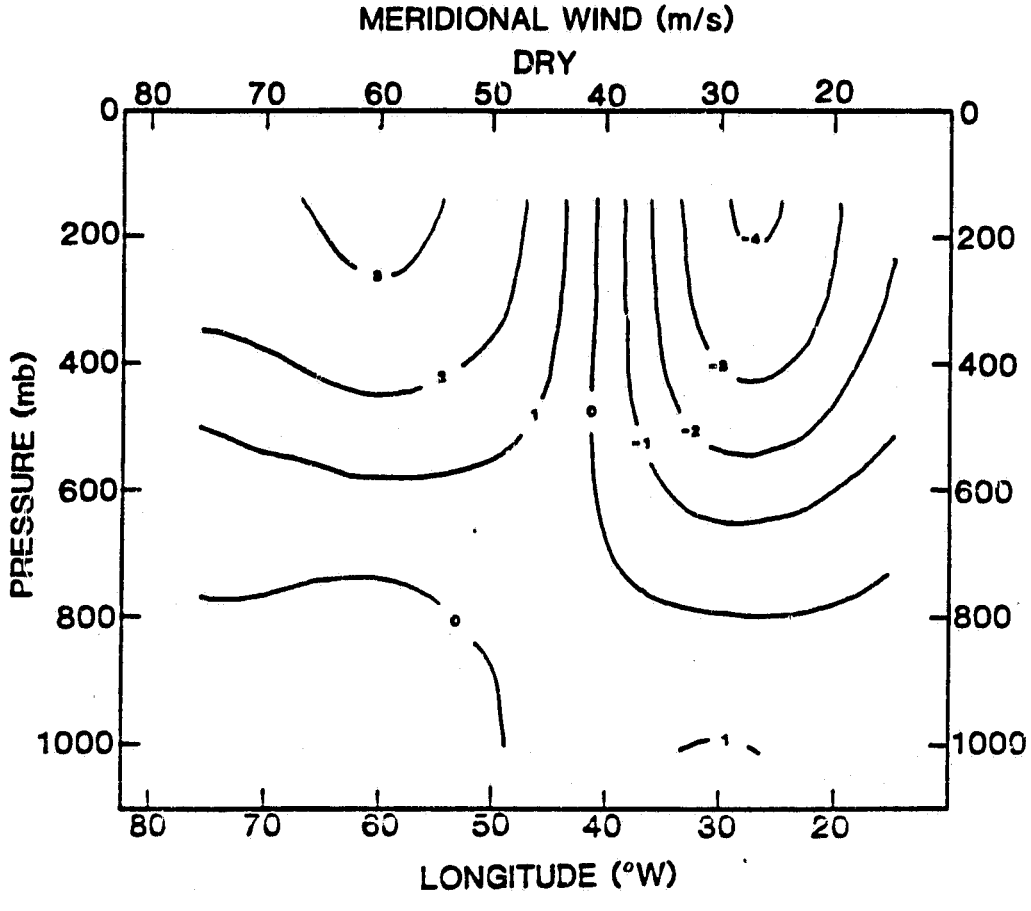
MERIDIONAL WIND (m/s)
DRY
80 70 60 50 40 30 20
0
200
400
600
800
1000
PRESSURE (mb)
LONGITUDE (°W)

Fig. 7b

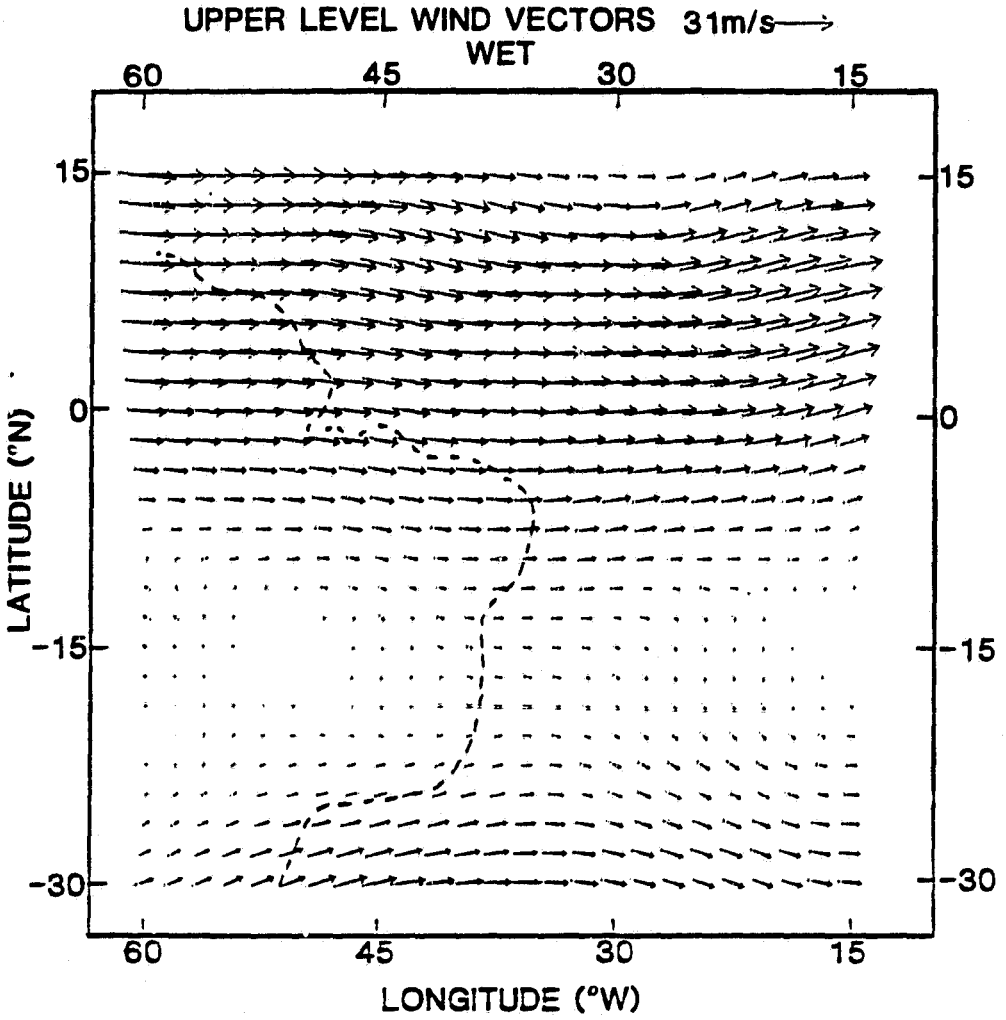
UPPER LEVEL WIND VECTORS 31m/s⟶
WET
60
45
30
15
15
0
-15
-30
LATITUDE (°N)
LONGITUDE (°W)

Fig 8a

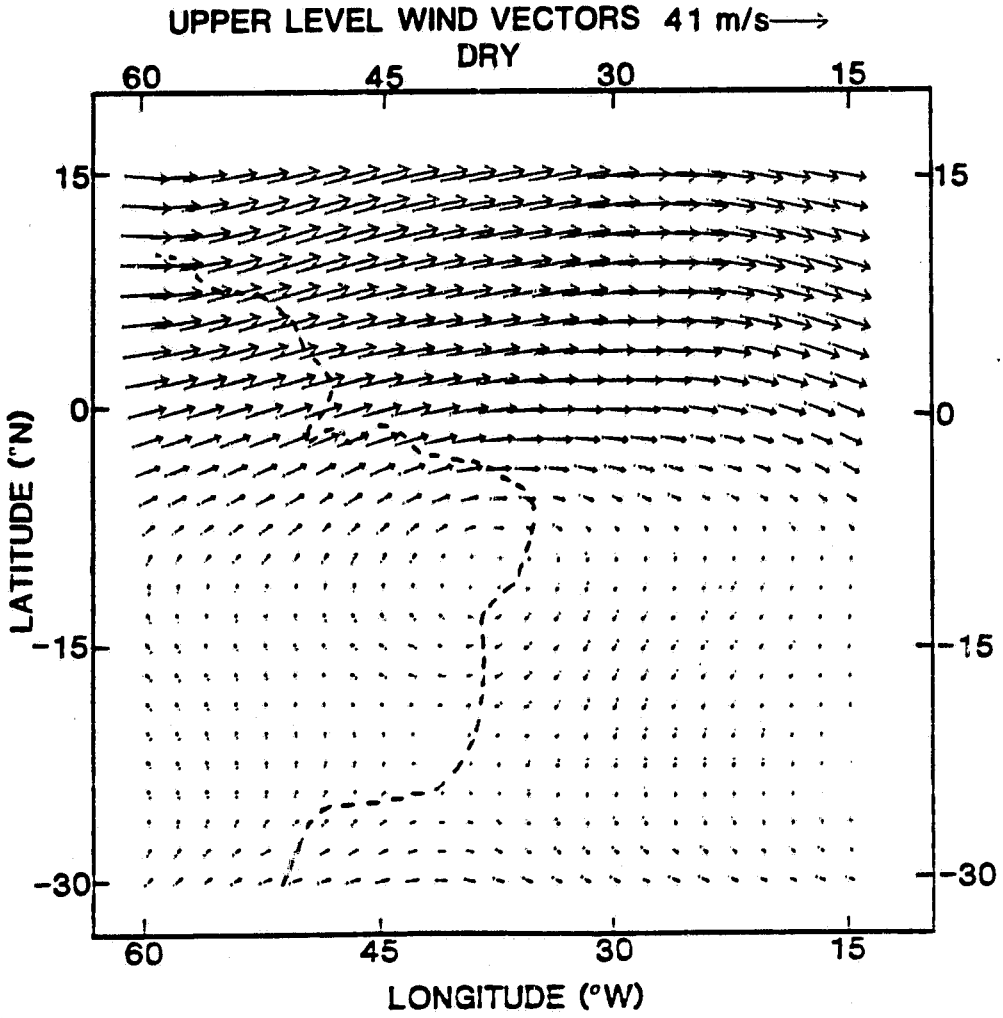
UPPER LEVEL WIND VECTORS 41 m/s⟶
DRY
60
45
30
15
15
0
-15
-30
LATITUDE (°N)
LONGITUDE (°W)

Fig 8b

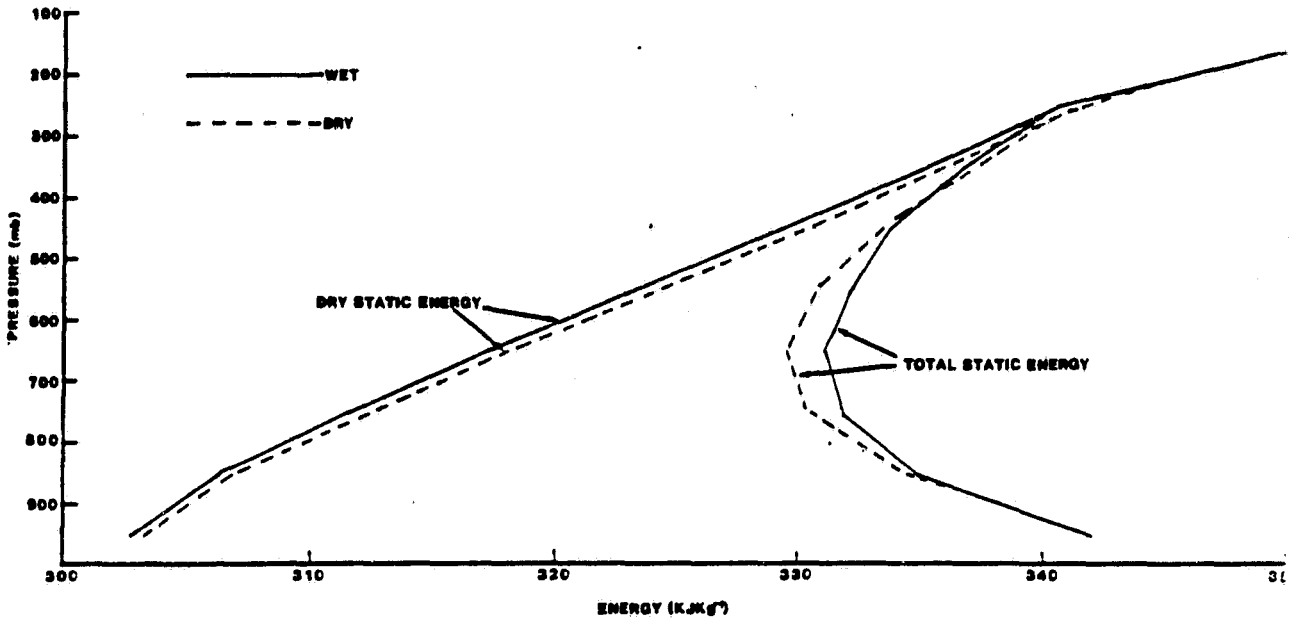
WET
DRY
DRY STATIC ENERGY
TOTAL STATIC ENERGY
PRESSURE (mb)
ENERGY (KJKg⁻¹)
300
310
320
330
340

Fig 9

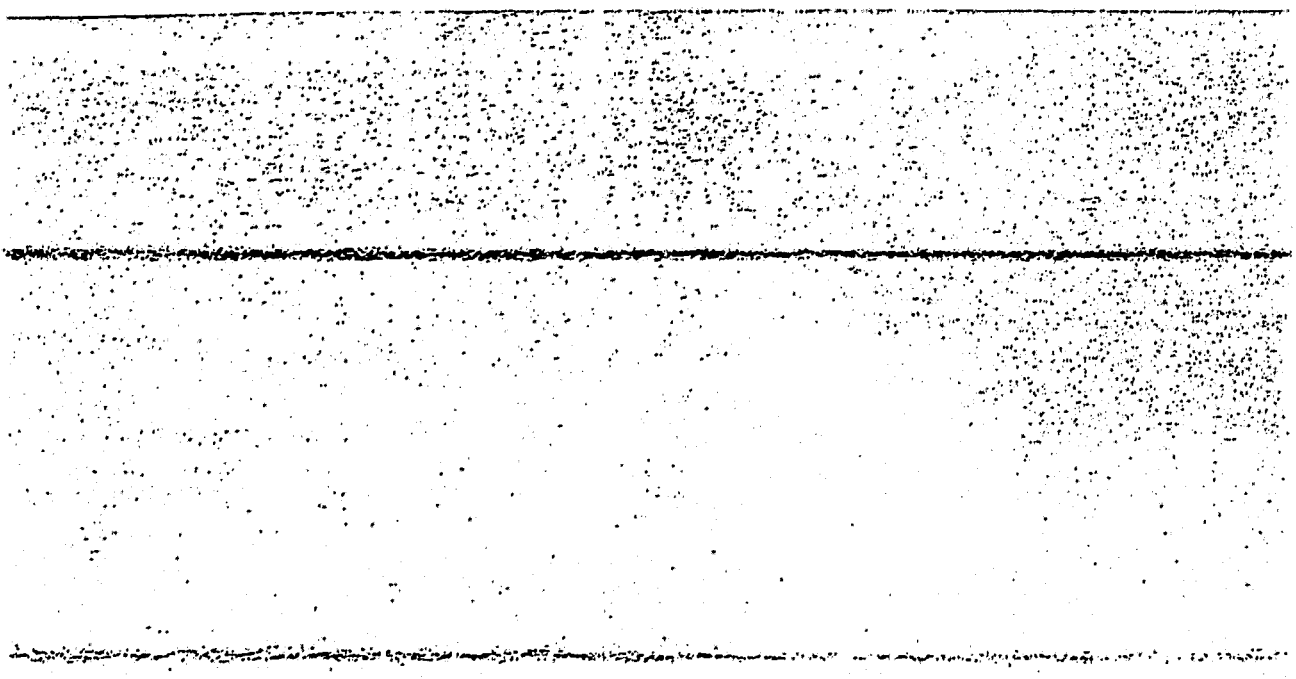

ORIGINAL PAGE IS
OF POOR QUALITY

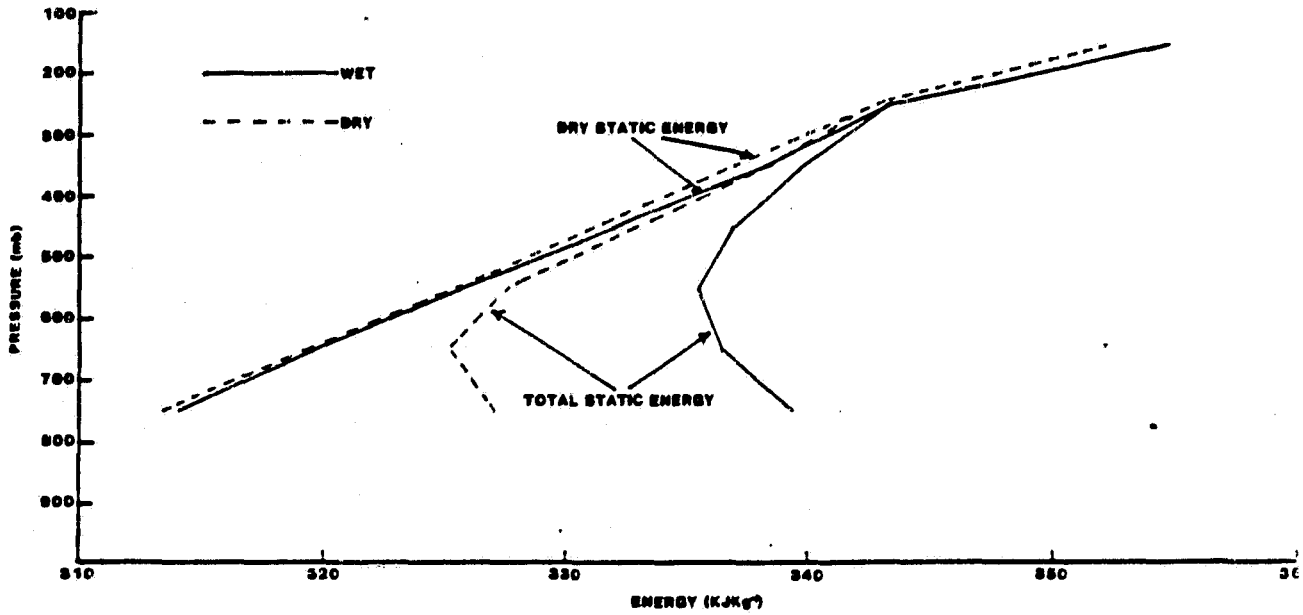

Fig. 10

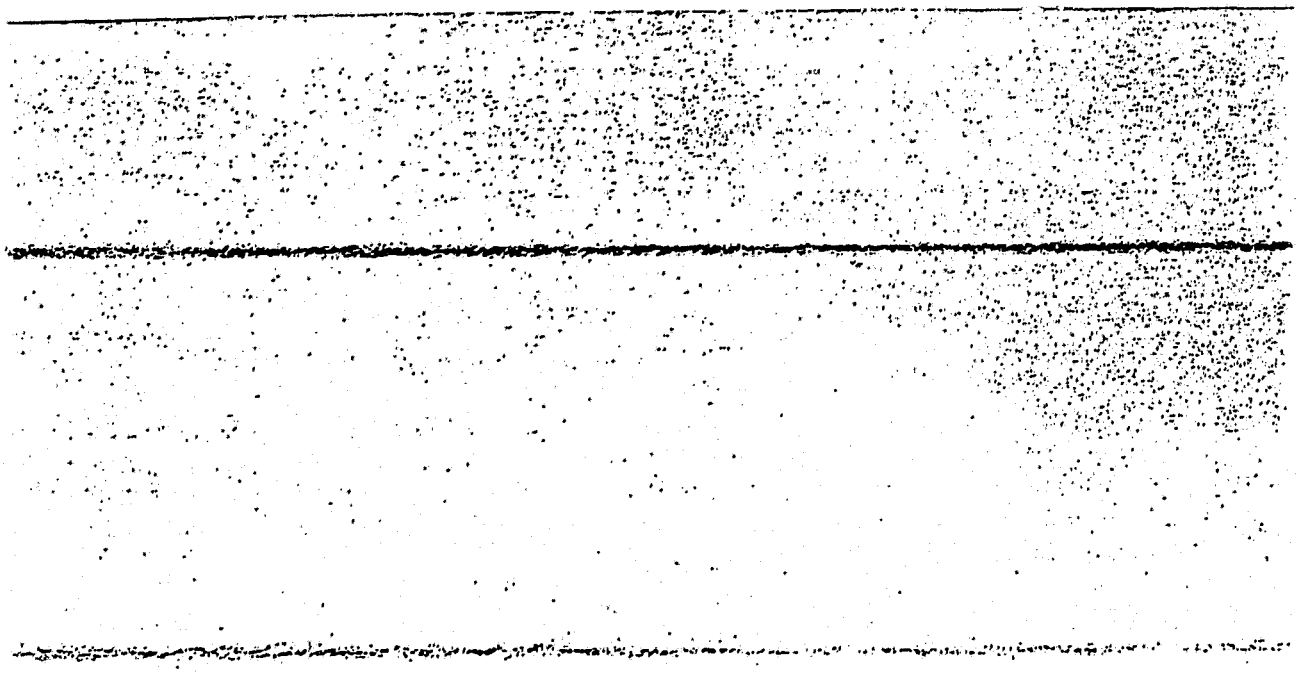

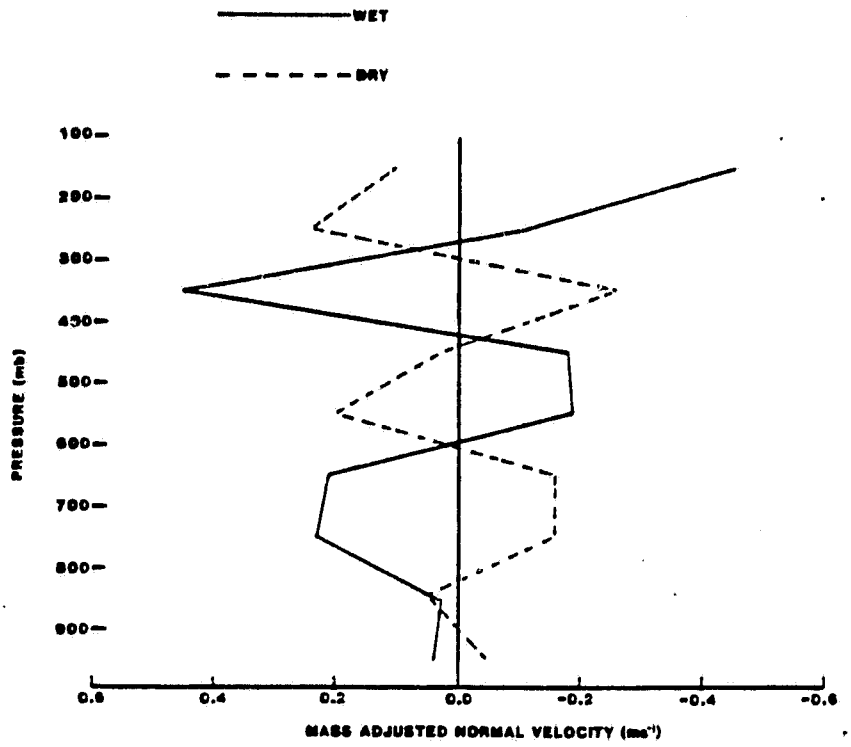
WET
DRY
100
200
300
400
500
600
700
800
900
PRESSURE (mb)
0.6
0.4
0.2
0.0
-0.2
-0.4
-0.6
MASS ADJUSTED NORMAL VELOCITY (ms⁻¹)

Fig. 11

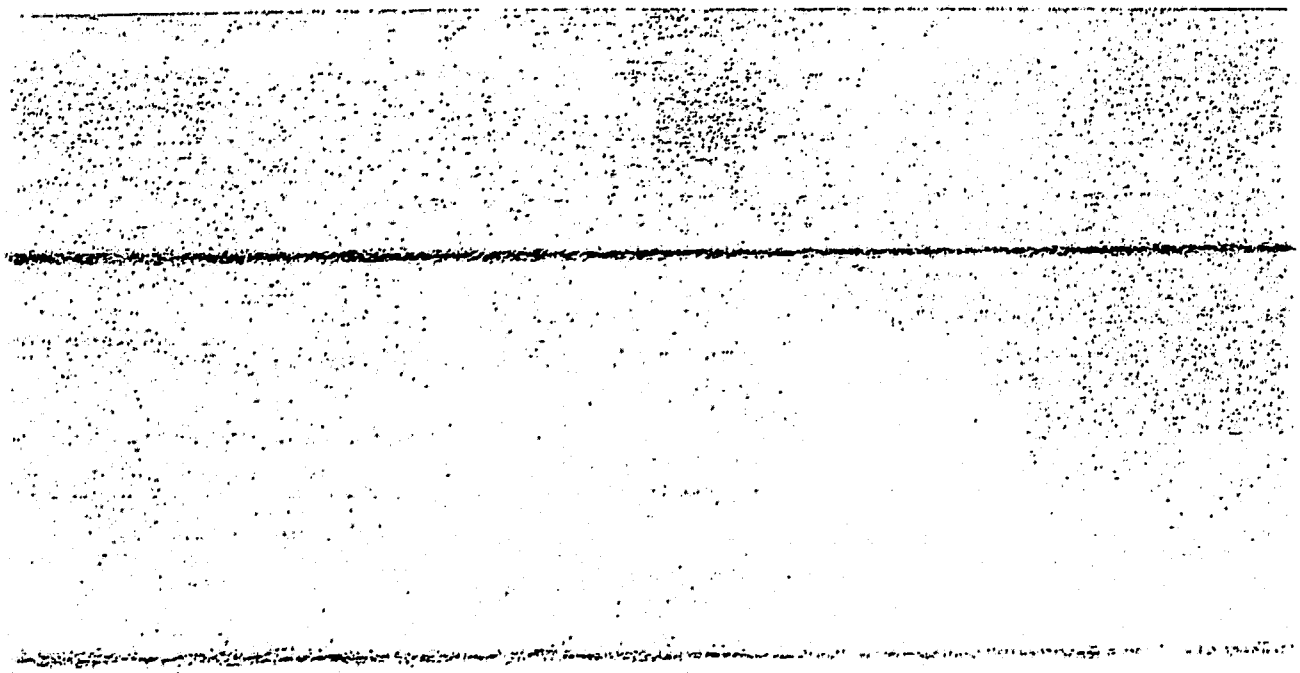

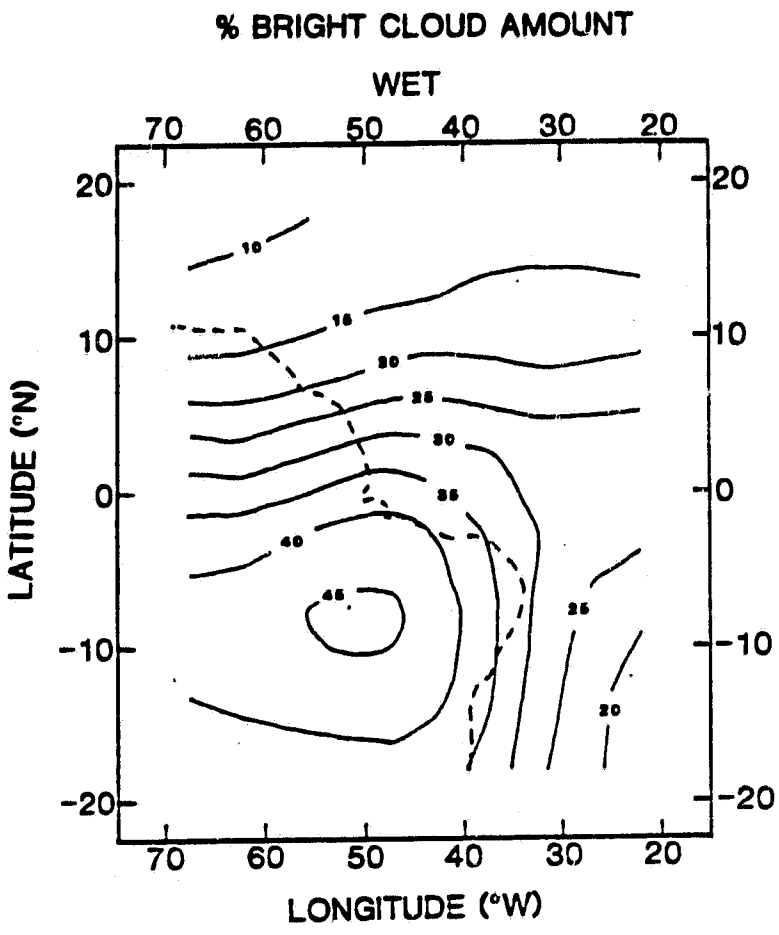
% BRIGHT CLOUD AMOUNT
WET
70 60 50 40 30 20
20
10
0
-10
-20
LATITUDE (°N)
LONGITUDE (°W)
10
15
20
25
30
35
40
45
25
20

Fig. 12a

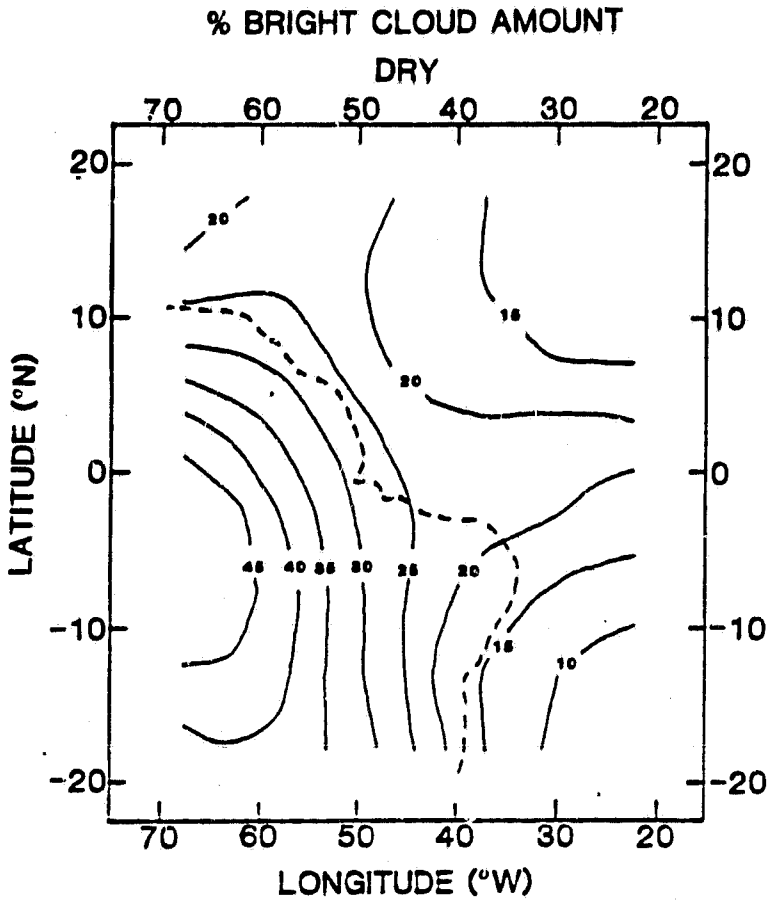
% BRIGHT CLOUD AMOUNT
DRY
70
60
50
40
30
20
20
10
0
-10
-20
LATITUDE (°N)
LONGITUDE (°W)
45
40
35
30
25
20
15
10

Fig. 12b

Table 1. Rainfall station list

Number	Station	Lat	Long	Altitude (m)
1.	Casa Nova	08°46′	41°14′	532
2.	Juazeiro	09°05′	40°06′	350
3.	Curaca	08°48′	39°40′	336
4.	Bodoco	07°32′	40°06′	605
5.	Ouricuri	07°50′	40°20′	444
6.	Petrolina	08°25′	40°47′	500
7.	Parnamirim	08°11′	40°03′	400
8.	Afranio	08°38′	41°09′	630
9.	Serrita	07°49′	39°29′	440
10.	Cabrobo	08°19′	39°37′	550
11.	Flores	08°04′	37°51′	561
12.	Souza	06°37′	38°20′	420
13.	Pombal	06°58′	37°47′	400
14.	Itaporanga	07°18′	38°10′	230
15.	Conceicao	07°21′	38°22′	470
16.	Teixeiro	07°13′	37°16′	770
17.	Princesa Isabel	07°44′	38°01′	660
18.	Sume	07°31′	36°58′	700
19.	Alexandria	06°25′	38°01′	315
20.	Patu	06°06′	37°38′	305
21.	Caico	06°40′	37°01′	190

Table 2. Normalized rainfall departures (a_j) and area averaged daily rainfall (mm) ($\overline{x}_j$)

	Feb. a_j	$\overline{x}_j$	Mar. a_j	$\overline{x}_j$	Apr. a_j	$\overline{x}_j$	May a_j	$\overline{x}_j$
1	-0.29	0.27	-0.31	0.14	0.03	3.64	0.00	3.29
2	0.74	12.24	-0.17	1.05	-0.25	0.61	-0.04	3.12
3	0.55	8.66	-0.32	0.00	-0.32	0.00	0.23	4.76
4	0.64	11.37	-0.06	3.46	-0.16	1.76	0.37	8.02
5	-0.28	0.63	0.45	9.26	-0.15	3.11	-0.06	1.94
6	-0.02	2.29	0.31	5.88	-0.19	0.97	0.05	2.99
7	0.28	5.05	-0.32	0.00	0.46	8.70	-0.21	1.24
8	0.80	12.98	-0.01	2.90	0.05	3.74	-0.05	1.48
9	0.00	3.71	-0.22	0.63	0.17	5.85	-0.12	1.85
10	-0.21	1.20	-0.08	3.45	-0.05	4.47	-0.31	0.00
11	-0.21	1.20	0.05	5.24	-0.32	0.00	-0.20	1.19
12	0.25	5.75	0.19	4.91	-0.25	0.67	-0.17	1.13
13	-0.09	1.27	0.65	13.66	-0.05	2.92	-0.30	0.22
14	0.02	2.20	0.28	5.58	-0.29	0.21	-0.31	0.04
15	-0.16	1.63	0.12	4.47	-0.32	0.00	-0.31	0.03
16	-0.24	0.68	0.37	5.65	-0.22	1.01	0.06	3.10
17	-0.10	2.21	0.08	4.46	-0.29	0.36	0.16	1.29
18	-0.25	0.62	-0.28	0.63	-0.29	0.26	0.14	3.59
19	-0.23	0.87	-0.32	0.00	-0.27	0.30	0.20	1.14
20	-0.09	2.11	-0.12	1.95	-0.27	0.36	-0.15	0.24
21	0.06	2.64	-0.28	0.33	0.38	6.47	-0.31	0.00
22	-0.32	0.00	-0.32	0.00	-0.14	1.41	-0.26	0.63
23	0.14	3.66	-0.32	0.00	-0.21	0.42	-0.31	0.00
24	0.61	11.69	-0.32	0.00	1.06	12.65	-0.31	0.00
25	0.10	4.39	-0.25	0.52	0.67	9.45	-0.31	0.19
26	0.79	10.15	-0.13	3.03	1.05	12.86	-0.10	1.67
27	0.07	4.52	0.23	3.92	-0.02	3.54	-0.31	0.00
28	-0.30	0.20	1.29	14.30	0.36	8.66	-0.31	0.00
			1.47	21.13	-0.23	1.35	-0.31	0.00
			0.21	5.00	-0.10	2.12	-0.31	0.00
			-0.16	2.38			-0.31	0.00

Table 3. Mean thermodynamic energy of the atmosphere ($KJKg^{-1}$)

Pressure layer (mb)	C_pT	ϕ	Lq	$C_pT+\phi$	Total
		a. Nordeste Wet			
SFC-900	297.2	5.5	39.2	302.7	341.9
900-800	291.4	15.0	28.4	306.4	334.8
800-700	286.1	25.4	20.2	311.6	331.8
700-600	280.3	37.1	13.8	317.4	331.1
600-500	273.1	50.4	8.6	323.5	332.1
500-400	263.3	66.1	4.3	329.4	333.7
400-300	250.3	84.8	1.5	335.1	336.6
300-200	232.0	108.5	0.0	340.5	340.5
200-100	208.9	142.3	0.0	351.2	351.2
		b. Nordeste Dry			
SFC-900	297.7	5.6	38.6	303.2	341.9
900-800	291.9	15.0	27.6	306.9	334.5
800-700	286.8	25.5	18.3	312.3	330.5
700-600	281.0	37.1	11.5	318.1	329.6
600-500	273.7	50.5	6.5	324.1	330.7
500-400	264.2	66.2	3.0	330.4	333.4
400-300	251.0	84.9	1.1	336.0	337.0
300-200	232.3	108.8	0.0	341.1	341.1
200-100	208.1	142.7	0.0	350.8	350.8
		c. Center Grid Wet			
SFC-900	999.9	999.9	999.9	999.9	999.9
900-800	999.9	999.9	999.9	999.9	999.9
800-700	288.5	25.6	25.3	314.1	339.4
700-600	282.3	37.3	16.9	319.7	336.5
600-500	274.9	50.8	9.8	325.6	335.4
500-400	265.5	66.6	4.7	332.0	336.8
400-300	253.0	85.3	1.4	338.2	339.6
300-200	234.2	109.0	0.0	343.2	343.2
200-100	211.5	143.1	0.0	354.6	354.6
		d. Center Grid Dry			
SFC-900	999.9	999.9	999.9	999.9	999.9
900-800	999.9	999.9	999.9	999.9	999.9
800-700	287.7	25.7	13.8	313.4	327.1
700-600	282.1	37.3	5.8	319.5	325.2
600-500	274.8	50.7	2.2	325.5	327.7
500-400	265.0	66.4	1.6	331.5	333.1
400-300	251.8	85.2	1.5	337.0	338.5
300-200	233.6	109.1	0.0	342.7	342.7
200-100	209.0	143.2	0.0	352.2	352.2

Table 4. Mean thermodynamic energy flux (x 10^{13} Js^{-1})

Pressure layer (mb)	$C_pT + \phi$	Lq	Total
	a. Nordeste Wet		
SFC-900	0.8	0.4	1.2
900-800	0.6	0.5	1.1
800-700	5.1	0.5	5.6
700-600	4.4	0.2	4.6
600-500	-4.4	-0.2	-4.5
500-400	-4.5	-0.1	-4.7
400-300	10.9	0.0	11.0
300-200	-2.7	0.0	-2.7
200-100	-11.2	0.0	-11.2
	b. Nodeste Dry		
SFC-900	-0.8	0.0	-0.8
900-800	1.1	0.2	1.2
800-700	-3.7	-0.2	-3.9
700-600	-3.8	-0.2	-3.9
600-500	4.9	0.0	5.0
500-400	0.5	-0.1	0.5
400-300	-6.0	0.0	-6.0
300-200	5.7	0.0	5.7
200-100	2.5	0.0	2.5